Tectonophysics 784 (2020) 228439

Contents lists available at ScienceDirect

Tectonophysics

journal homepage: www.elsevier.com/locate/tecto

Low-temperature thermochronology of the South Atlantic margin along Uruguay and its relation to tectonic events in West Gondwana

João Pacífico Silveira Luiz Machado[a,b,*], Andréa Ritter Jelinek[b], Randell Stephenson[a], Claudio Gaucher[c], Marcos Müller Bicca[b], Leticia Chiglino[c], Frederico Antonio Genezini[d]

[a] School of Geosciences, University of Aberdeen, United Kingdom
[b] Instituto de Geociências, Universidade Federal do Rio Grande do Sul, Porto Alegre, Brazil
[c] Facultad de Ciencias, Universidad de la República, Montevideo, Uruguay
[d] Instituto de Pesquisas Energéticas e Nucleares, Centro do Reator de Pesquisas, São Paulo, Brazil

ARTICLE INFO

Keywords:
Thermochronology
Fission-tracks
(U−Th)/He
West Gondwana
South Atlantic
Uruguay

ABSTRACT

The geodynamic forces acting during Jurassic-Cretaceous South Atlantic rifting provoked intense transformations in West Gondwana, such as the reactivation of ancient basement structures, voluminous magmatism and general uplift of the new continental margins. Low-temperature thermochronology records cooling associated with uplift *syn*- and post-breakup along the Brazilian margin, while further south, in Uruguay, mostly pre-breakup uplift is identified. Thermochronometry data are scarce in Uruguay, but previous studies suggest that basement cooling and exhumation preceded West Gondwana breakup by hundreds of millions of years. To improve our knowledge of Uruguay's thermotectonic evolution, in this study we present 19 apatite fission-track ages, 42 apatite and 40 zircon (U−Th)/He single crystal ages for the Uruguayan shield (UYS), from which we modeled 19 inverse thermal histories. Our results suggest that the UYS temperatures were below 200 °C since the early Paleozoic, and that cooling below 110 °C started during the Carboniferous, with continuous exhumation of the basement until Early Cretaceous. The onset of this long-term uplift is correlated with orogenesis and terrane accretions in the SW margin of West Gondwana during the Paleozoic. Lithosphere thinning and uplift preceding breakup contributed to the continuous Late Paleozoic to middle Mesozoic exhumation, until the voluminous volcanism of the Paraná-Etendeka Large Igneous Province (*c.* 133 Ma). This magmatic event, combined with the thermal influence of the Tristão da Cunha mantle plume and rift spreading, likely raised the basement geotherm during the Late Cretaceous. Models suggest a slight increase in temperatures of the UYS from Late Cretaceous until the Oligocene, when a final cooling to surface temperatures took place. Our findings corroborate a long and complex thermal history for Uruguay, with crustal uplift occurring essentially before West Gondwana breakup.

1. Introduction

The Atlantic passive margin of South America was established after Gondwana breakup in the Jurassic-Cretaceous, during which rifting propagated from southernmost Tierra del Fuego towards the N, forming the eastern continental margins of Argentina, Uruguay and Brazil (*e.g.* Nürnberg and Müller, 1991; Pérez-Díaz and Eagles, 2014). Basement uplift *syn*- and post-rift have been widely reported by low-temperature thermochronometry studies in SE Brazil (*e.g.* Gallagher et al., 1994, 1995; Gallagher and Brown, 1999; Tello Saenz et al., 2003; Hackspacher et al., 2004; Cogné et al., 2011, 2012; Karl et al., 2013; Krob et al., 2019; Van Ranst et al., 2019), where the high escarpments (up to 2.000 m) from the Serra do Mar and Serra da Mantiqueira provide an ideal scenario for this research method. According to these studies, cooling in the region is associated with uplift and exhumation, often related to the far-field effects of the Andean Orogeny and to structural reactivations in the passive margin during the development of the Atlantic Ocean. On the other hand, thermochronometry studies are scarcer towards the south of the Atlantic margin, where a subdued topography and low relief are dominant. Published data suggest that an important limit between pre- and post-rift cooling and exhumation is located in the Florianópolis region, southern Brazil (Fig. 1), where a very complex thermal history has been reported (Jelinek et al., 2003; Karl et al., 2013; Hueck et al., 2018a). Further south of this region, thermochronometry studies have reported mainly pre-rift Paleozoic cooling phases in southernmost Brazil (Borba et al., 2002, 2003;

* Corresponding author at: School of Geosciences, University of Aberdeen, United Kingdom.
E-mail addresses: j.luizmachado.18@abdn.ac.uk, joao.machado@ufrgs.br (J.P. Silveira Luiz Machado).

https://doi.org/10.1016/j.tecto.2020.228439
Received 5 November 2019; Received in revised form 28 March 2020; Accepted 3 April 2020
Available online 08 April 2020
0040-1951/

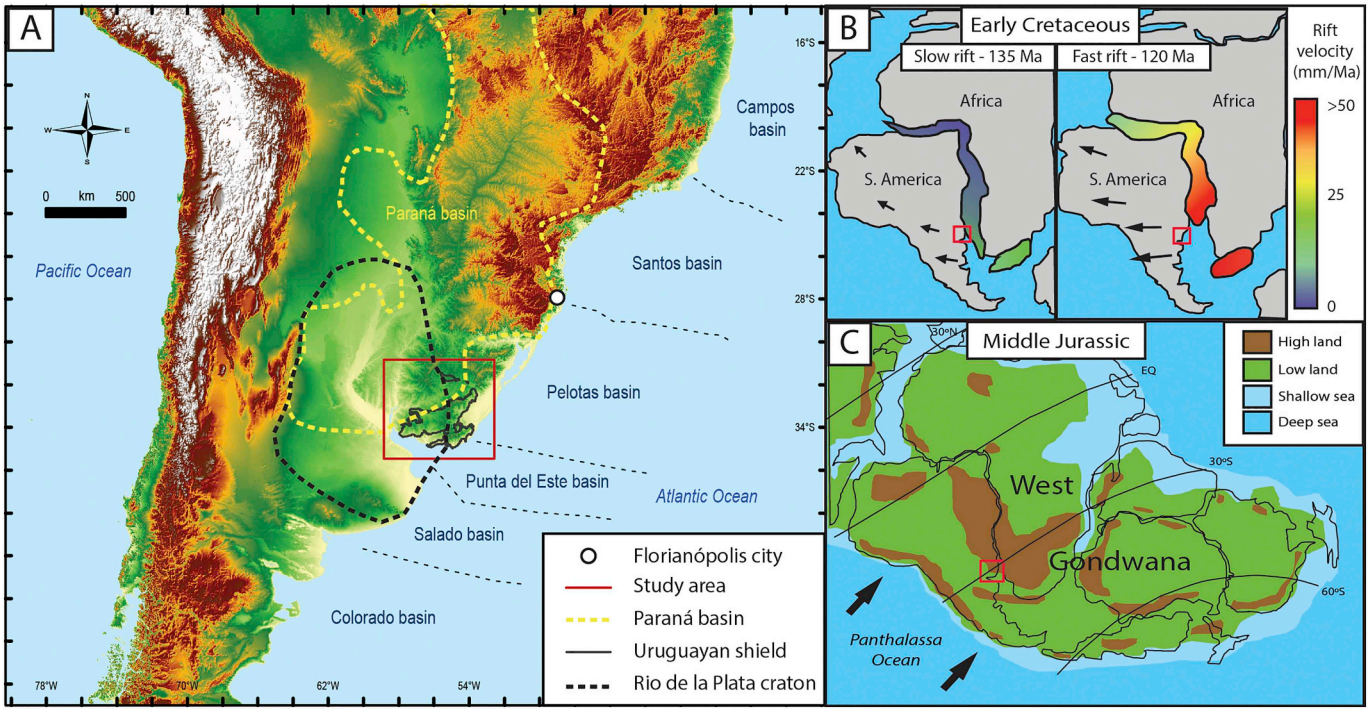

Fig. 1. Panel with (A) DEM image of the study area in the South Atlantic margin, with schematic boundaries of the Paraná Basin and Rio de La Plata Craton indicated. The region of Florianópolis marks the limit between pre-rift cooling (south) and post-rift cooling (north); (B) study area location during the South Atlantic rift velocity increase (after Brune et al., 2016) and (C) before West Gondwana break-up, with subduction of the Panthalassa Ocean under West Gondwana (after Scotese et al., 1999).

Oliveira et al., 2016; Machado et al., 2019), Uruguay (Kollenz, 2015; Hueck et al., 2017; Gomes and Almeida, 2019) and Argentina (Kollenz et al., 2017). These were generally linked to Paleozoic orogenic cycles on the active SW margin of Gondwana and the geodynamics of Gondwana breakup.

Approximately 800 km south of Florianópolis, Uruguay has been the focus of thermochronometry studies in recent years, but data are still very limited in the region. The Uruguayan shield (UYS) occupies almost half of the territory of Uruguay (Figs. 1 and 2) and includes exposures of the Archean to Paleoproterozoic Rio de La Plata Craton and of the Neoproterozoic Dom Feliciano Belt, associated with the formation of West Gondwana (Hartmann et al., 2001; Gaucher et al., 2011; Oyhantçabal et al., 2011). Although passive margins and cratons are often considered as characterized by long-term stability, the low-temperature thermochronology studies in Uruguay indicate basement cooling since the early Paleozoic, suggesting a lengthy and complex Phanerozoic thermotectonic history. Available thermochronometry data suggest that the main exhumation event in the region was initiated well before Gondwana breakup (Kollenz, 2015; Hueck et al., 2017; Gomes and Almeida, 2019). However, the current thermal histories modeled for the UYS are based on distinct thermochronometers (*i.e.* apatite fission tracks or (U−Th)/He in apatites and zircons) and suggest alternative phases of cooling and reheating of the basement, implying in somewhat conflicting geodynamic models for the regional tectonic evolution (see Kollenz, 2015; Hueck et al., 2017; Gomes and Almeida, 2019). The complex and scattered thermochronometry data in the region limit our understanding of the tectonic activity preceding South Atlantic rifting and breakup.

A deeper comprehension of the cooling and exhumation history of the Uruguay basement can improve our models for the Gondwana breakup and tectonic activity in the early stages of rifting. Moreover, it is necessary to evaluate the somewhat conflicting models for exhumation of the UYS. Therefore, aiming to enhance our knowledge of the thermal history of the region, in this work we combine the methods used individually in previous thermochronometry studies and provide new thermal models for the Uruguayan basement. We present a new dataset with 19 apatite fission-track ages, 42 apatite and 40 zircon (U−Th)/He single crystal ages, from which we model 19 inverse thermal histories across the UYS. After integration with previously published data, we identify the main cooling/reheating phases of the shield and associate them to the collisional cycles in the SW margin of Gondwana, and to the opening of the South Atlantic. Our results support models of a complex long-lived thermal evolution for the Uruguayan shield, and a thermotectonic history that utilizes the thermochronometry data currently available for the region is suggested.

2. Geological context

Uruguay is located at the eastern margin of South America and exhibits a surprising geological diversity considering its relatively small size. Its Precambrian basement records geological events from the Archean and outcrops in about half of the country's territory (Hartmann et al., 2001; Masquelin, 2006), which presents low topography and subdued relief, with very few peaks over 500 m. The Uruguayan shield crops out mainly in the southern and eastern part of the country, and is divided into four tectonostratigraphic terranes, while the remaining area is covered by Phanerozoic volcano-sedimentary deposits (Fig. 2).

2.1. The Uruguayan shield (UYS)

The four UYS terranes are separated by regional shear zones and are known, from W to E, as the: 1) Piedra Alta Terrane (PAT), 2) Tandilia Terrane (TT), 3) Nico Pérez Terrane (NPT), and 4) Cuchilla Dionisio Terrane (CDT) (Bossi and Gaucher, 2004, 2014a; Bossi and Cingolani, 2009). Although this division is still a matter of debate, the westernmost PAT and TT are unanimously considered part of the Rio de la Plata Craton, a major tectonic feature in South America; the easternmost CDT is part of the Dom Feliciano Belt and has been associated with the Kalahari Craton, of southern Africa; and the central and highly complex NPT has been considered part of the Rio de La Plata Craton or not,

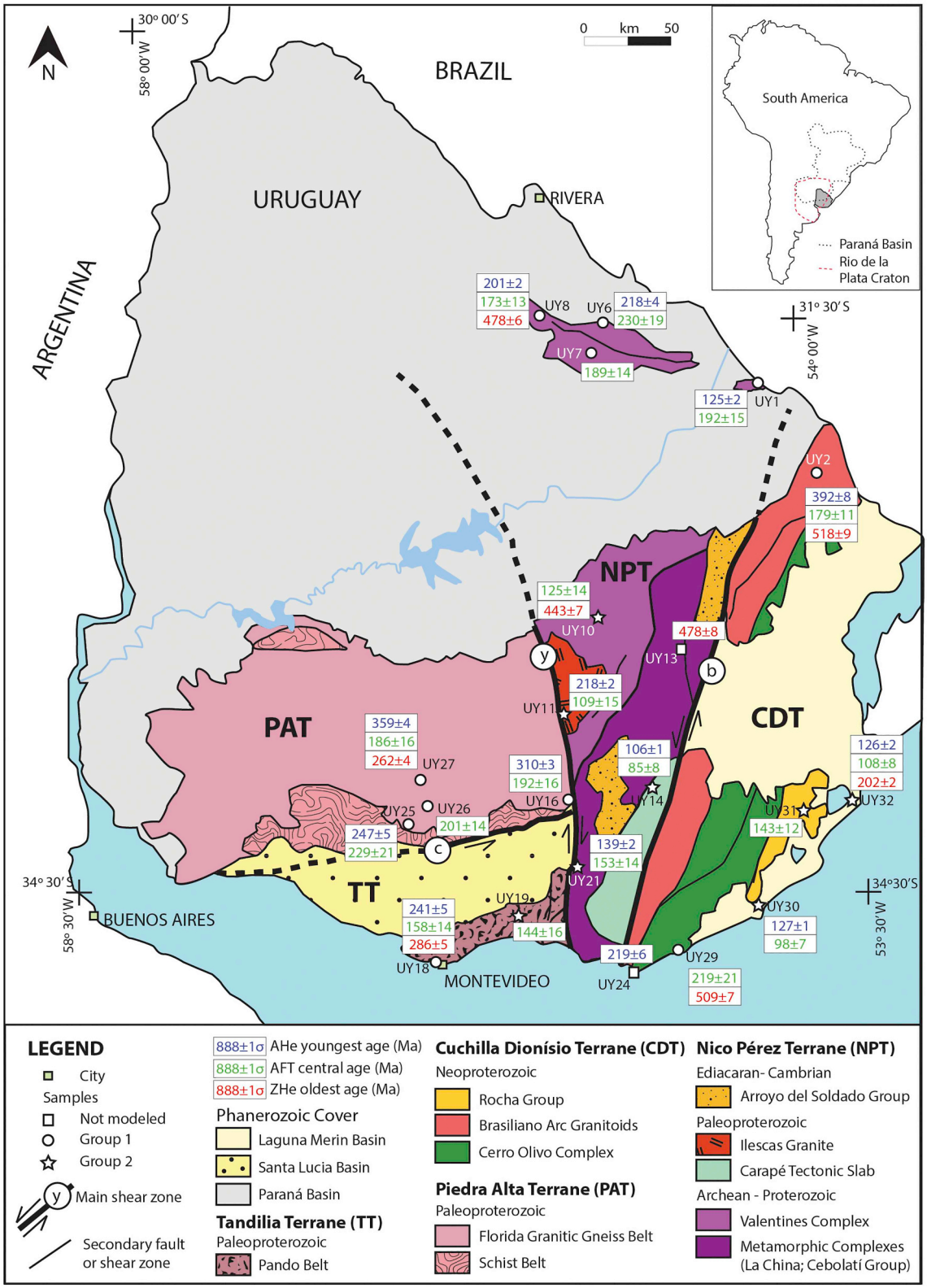

Fig. 2. Simplified geological map of Uruguay with sample locations and new thermochronometry ages. For a clearer view, only the central AFT ages, oldest ZHe and youngest AHe single crystal ages are reported here. For a more comprehensive evaluation of the (U−Th)/He ages and their dispersion see Tables 3 and 4, and Sections 4.2, 4.3 and 5.1. For the discussion about the model groups see Sections 4.4 and 5.2. Main shear zones: (c) Colonia, (y) Sarandí del Yí and (b) Sierra Ballena. Inset map indicates the approximated extension of the Paraná Basin and Rio de la Plata Craton. Adapted after Bossi and Ferrando (2001).

depending on author (see Basei et al., 2005; Bossi and Gaucher, 2004; Gaucher et al., 2011; Hartmann et al., 2001; Masquelin, 2006; Oriolo et al., 2016a; Oyhantçabal et al., 2018; Philipp et al., 2016; Rapela et al., 2011; Santos et al., 2017). In any case, there is consensus that all terranes were finally assembled during the end of the Brasiliano/Pan-African Orogeny (Neoproterozoic), a multi-episodic collision between

the Rio de la Plata, Congo and Kalahari cratons and several microcontinents and arc terranes, which culminated with the consolidation of West Gondwana (Gaucher et al., 2009a, 2011; Hueck et al., 2018b; Philipp et al., 2018; Schmitt et al., 2018).

Three major crustal-scale regional shear zones delimit the four UYS terranes, and several N*E*-trending smaller lineaments occur in the NPT and CDT. The oldest lineament is the Colonia Shear Zone, which separates the PAT from the TT (Bossi and Cingolani, 2009). It is an E-W trending, several km-thick ultramylonite band, showing abundant sinistral shear indicators (Ribot et al., 2005; Abre et al., 2014). The age of the shear zone has been determined by moscovite K−Ar ages of deformed granitoids as 1.72 Ga (Faraone, 2018). Central in the shield, the Sarandí del Yí Shear Zone is a mylonitic belt with *c.* 2 km width and a NNW-SSE strike, which displays dextral shearing with sinistral reactivation and limits the western PAT and TT from the central NPT (Bossi and Gaucher, 2014a; Oriolo et al., 2018). Ar−Ar ages of mafic dikes deformed by the main dextral shear yielded Mesoproterozoic ages of *c.* 1.20 Ga (Teixeira et al., 1999), that have been related to the tangential collision between the TPA and TT with the NPT during the formation of the Rodinia supercontinent (Bossi and Cingolani, 2009; Gaucher et al., 2011; Bossi and Gaucher, 2014a). More recent publications have supported a Neoproterozoic onset of deformation (*c.* 630 Ma), linked to the collision of the Rio de la Plata and Congo cratons during West Gondwana formation (Rapela et al., 2011; Oriolo et al., 2016b, 2018), but the new ages do not rule out a Mesoproterozoic main event (Santos et al., 2017). This discussion is still ongoing and has important implications for the Precambrian evolution of Uruguay. Another major lineament is the Sierra Ballena Shear Zone, a *c.* 4 km-wide mylonitic belt with NNE-SSW direction that propagates to southernmost Brazil as the Dorsal do Canguçu Shear Zone (Fernandes et al., 1993; Fernandes and Koester, 1999; Oriolo et al., 2018). In Uruguay this shear zone represents the suture between the central NPT and the coastal CDT, and displays sinistral shearing during the end of the Brasiliano/Pan-African Orogeny (latest Ediacaran-Cambrian) with brittle reactivation during the Mesozoic (Bossi and Gaucher, 2004, 2014a; Hueck et al., 2017; Oriolo et al., 2018).

The PAT is a Paleoproterozoic (2.2 to 2.0 Ga) block composed of two supracrustal low-grade metamorphic belts (Arroyo Grande and San José belts), separated by the wide central Florida Belt, which comprises granitoids and gneiss (Hartmann et al., 2001; Oyhantçabal et al., 2011; Bossi and Piñeyro, 2014). The southern San José Belt is cut by the E-W Colonia Shear Zone and partially covered by the Santa Lucía Basin. The central Florida Belt was intruded by thousands of mafic dikes with E-W direction around 1.79 Ga (Teixeira et al., 1999) which underwent a NW-SE flexure near the Sarandí del Yí Shear Zone, indicating dextral movement during the collision of the PAT and the NPT (Bossi and Campal, 1992; Hartmann et al., 2001; Gaucher et al., 2011; Bossi and Piñeyro, 2014; Oriolo et al., 2016b; Oyhantçabal et al., 2018).

The TT, to the south of the Colonia Shear Zone, comprises the Paleoproterozoic Montevideo Formation (Pando Belt) and several intrusive granitoids. The terrane continues to the south beneath the Río de la Plata and into Argentina, cropping out again in its type area in the southern Buenos Aires Province, Argentina (Bossi and Cingolani, 2009). Apart from older ages for the metasediments and intrusive granitoids compared to the PAT, Nd model ages are in average 200 Myr older in the TT (Pamoukaghlián et al., 2017), matching comparable model ages in the type area in Argentina (Hartmann et al., 2002). Furthermore, Neoproterozoic anorogenic granitoids and sedimentary rocks occur in the TT in Argentina and Uruguay (Gaucher et al., 2008; Abre et al., 2014) but are so far unknown in the PAT.

The NPT (Bossi and Campal, 1992) is a complex terrane in Uruguay and a key element for understanding the formation of West Gondwana. It is usually considered part of the Rio de la Plata Craton since the Mesoproterozoic (Hartmann et al., 2001; Gaucher et al., 2008, 2009b; Bossi and Cingolani, 2009; Santos et al., 2017), but other studies have related the NPT to the Congo Craton and the Dom Feliciano Belt, suggesting it was amalgamated to the Rio de la Plata Craton only during the Ediacaran (Oyhantçabal et al., 2011; Rapela et al., 2011; Oriolo et al., 2016a). The NPT presents a highly complex geology and the oldest rocks in Uruguay, with major internal units limited by the NE-SW shear zones, a basement window (Isla Cristalina de Rivera) cropping out far north in the Paraná Basin (Fig. 2), and continuity to southernmost Brazil (Taquarembó Terrane) (Oyhantçabal et al., 2011, 2012; Bossi and Gaucher, 2014b; Oriolo et al., 2016a, 2018). Moreover, the NPT was strongly reworked in the Brasiliano/Pan-African Orogeny, including the intrusion of several granites (Oyhantçabal et al., 2011; Oriolo et al., 2016a, 2016b). In a simplified way, the NPT is composed of the Valentines Granulitic Complex in the northwest, the La China Complex and the Cebolatí Group in the middle, and the Carapé Tectonic Slab and Mesoproterozoic volcano-sedimentary successions in the southeast. The Valentines Complex, comprises gneisses, pyroxenites and banded iron formations as well as intruding tonalites, trondhjemites and granites with ages between 2.6 and 2.2 Ga (Santos et al., 2003; Oyhantçabal et al., 2012). They are in turn intruded by the Illescas rapakivi granite, which yielded an U−Pb zircon age of 1.78 Ga (Bossi and Cingolani, 2009). The central domain includes the La China Complex, which comprises metatonalites of amphibolite facies, and the metasedimentary Cebollatí Group (Las Tetas complex), both units with Archean ages between 3.4 and 2.7 Ga (Hartmann et al., 2001; Gaucher et al., 2010, 2011, 2014). At the southeastern corner of the NPT, the Carapé Complex (Campanero Unit), is a tectonic slab emplaced in the NPT in the latest Ediacaran-early Cambrian, and comprises mainly metagranitoids and metasediments juxtaposed by reverse and transcurrent faults (Hartmann et al., 2001; Mallmann et al., 2007; Chiglino et al., 2010; Bossi et al., 2014). Unconformably overlying parts of the NPT are remnants of the Arroyo del Soldado Group, a 5.000 *m* thick marine platform succession rich in carbonate deposits and with depositional age between 566 and 530 Ma (Gaucher, 2000; Gaucher et al., 2004; Blanco et al., 2009). Last, the youngest volcanic rocks so far described in Uruguay are located in the NPT: subalkaline rhyolites with U−Pb SHRIMP ages of 77 ± 1 Ma (Gaucher et al., 2016). This volcanism can be related to the Meso-Cenozoic alkaline magmatism spread around the Paraná Basin and linked to a long-lived process of mantle upwelling in the region (Riccomini et al., 2005).

The CDT, also known as Punta del Este Terrane (Oyhantçabal et al., 2011), is an allochthonous unit laterally accreted to the NPT during the Brasiliano/Pan-African Orogeny (Bossi and Gaucher, 2004). This terrane is composed mainly of deformed calc-alkaline granites (Aiguá and Cuchilla Dionisio batholiths) with ages between 615 and 530 Ma, and continues in Brazil as the Pelotas Batholith (Fernandes et al., 1995; Bossi and Gaucher, 2004; Philipp et al., 2016). The Paleo-Mesoproterozoic Cerro Olivo Complex occurs further east in the terrane and is considered its basement, including high-grade metamorphic rocks with protolith ages between 1.000 and 750 Ma, metamorphosed at *c.* 650 Ma (Bossi and Gaucher, 2004; Basei et al., 2011; Oyhantçabal et al., 2011; Peel et al., 2018; Will et al., 2019). Finally, near the South Atlantic coast the metasediments of the Rocha Group are exposed. These have ages between *c.* 600 to 550 Ma and affinity to units from the Kalahari Craton, being correlated to the Oranjemund Group of the Gariep Belt in Namibia (Bossi and Gaucher, 2004; Basei et al., 2005).

Although the discussion is still ongoing on how and when the tectonostratigraphic terranes of the UYS were assembled, there is a consensus that the long lived Brasiliano/Pan-African Orogeny represents the final event for the consolidation of Uruguayan basement. The juxtaposition of UYS terranes, related to the diachronous collision of Uruguayan, Brazilian and African units, led to the formation of the West Gondwana megacontinent by Cambrian times (Bossi and Gaucher, 2004, 2014a). The successive collisions were responsible for establishing sutures that later played an important role during Pangea breakup and South Atlantic opening in the Mesozoic (Oriolo et al., 2018; Schmitt et al., 2018; Will and Frimmel, 2018).

Table 1
Details of each location and analysis made. Stratigraphic ages from Bossi & Gaucher (2004) and Masquelin (2006); coordinates in degrees and datum WGS84; (D. sea) is the shortest distance to the Atlantic Ocean.

Sample	Lithology	Age (Ma)	Lat (∘)	Long (∘)	Altitude (m)	D. sea (km)	Analysis
UY1	Granite	> 550	-31.89	-54.16	225	181	AFT, AHe
UY2	Granite	575 + 14	-32.35	-53.79	110	133	AFT, AHe, ZHe
UY6	Granite	590-530	-31.59	-55.10	259	277	AFT, AHe
UY7	Granite	550-510	-31.75	-55.18	208	278	AFT
UY8	Granite	590-530	31.55	-55.49	193	312	AFT, AHe, ZHe
UY10	Granite	> 1000	-33.12	-55.13	245	173	AFT, ZHe
UY11	Granite	590-530	-33.61	-55.33	235	161	AFT, AHe
UY13	Granite	> 1000	-33.28	-54.62	102	120	ZHe
UY14	Granite	590-530	-33.99	-54.78	131	89	AFT, AHe
UY16	Granite	*c.*2200	-34.06	-55.31	266	104	AFT, AHe
UY18	Gnaisse	*c.*2200	-34.92	-56.17	150	111	AFT, AHe, ZHe
UY19	Granite	2054 + 11	-34.67	-55.64	55	69	AFT
UY21	Granite	574 + 34	-34.41	-55.25	182	66	AFT, AHe
UY24	Gnaisse	1006 + 37	-34.97	-54.95	9	0	AHe
UY25	Diorite	2065 + 9	-34.19	-56.32	54	153	AFT, AHe
UY26	Granite	*c.*2100	-34.10	-56.20	47	150	AFT
UY27	Granite	*c.*2200	-33.96	-56.24	133	163	AFT, AHe, ZHe
UY29	Granite	> 550	-34.85	-54.63	7	0	AFT, ZHe
UY30	Schist	< 1540	34.59	-54.12	3	0	AFT, ZHe
UY31	Granite	556 + 7	-34.11	-53.85	71	17	AFT
UY32	Granite	678 + 14	-34.04	-53.54	4	0	AFT, AHe, ZHe

2.2. Phanerozoic cover

Most of the territory of Uruguay is covered by remnants of three Phanerozoic basins: the continentally wide intracratonic Paraná Basin, locally named the Norte Basin, and the South Atlantic rift related Laguna Merin and Santa Lucia basins (Fig. 2).

The Paraná Basin, which spreads over Argentina, Brazil, Paraguay and Uruguay, was developed in the interior of West Gondwana during Paleozoic and Mesozoic times. Depositional packages within this basin are divided into six supersequences separated by interregional unconformities: Rio Ivaí (Ordovician to Silurian), Paraná (Devonian), Gondwana I (Upper Carboniferous to Lower Triassic), Gondwana II (Middle to Upper Triassic), Gondwana III (Jurassic to Lower Cretaceous), and Bauru (Upper Cretaceous) (Milani, 1997; Milani et al., 2007). The SE margin of the Paraná Basin lies within Uruguay (Fig. 1), where basinal deposits cover most of the NW of the country and are associated with the supersequences Paraná, Gondwana I and Gondwana III, reaching a maximum thickness between 2.300 and 3.000 m (De Santa Ana et al., 2006). The lowermost deposits correspond to the Devonian Durazno Group, cropping out at the SE margin of the basin and related to the Paraná Supersequence. This group comprises a transgressive-regressive siliciclastic sequence of shallow marine deposits, with paleocurrents to the NW and sourced from the UYS terranes, being deposited within an extensional subsidence regime (Sprechmann et al., 1993; Uriz et al., 2016). Separated by an unconformity, the overlying Gondwana I Supersequence represents a transgressive-regressive cycle as well. It comprises latest Carboniferous to Permian deposits that record the transition from glaciolacustrine, to marine and finally fluvial and aeolian environments (De Santa Ana et al., 2006; Beri et al., 2011). Last, unconformably above these, lies the continental deposits of the Gondwana III Supersequence, which comprises fluvial and aeolian formations capped by basalt flows from the Paraná-Etendeka Large Igneous Province (LIP) (Sprechmann et al., 1981), with eruption peak at *c.* 133 Ma and related to the Tristão da Cunha mantle plume and the opening of the South Atlantic (Turner et al., 1994; Rossetti et al., 2014; Cernuschi et al., 2015).

The tectonic stress associated with the Pangea breakup and Atlantic opening led to the development of the Santa Lucia and Laguna Merin basins onshore, which form a ENE-WSW corridor known as SaLAM, that is considered an aborted rift precursor to the opening of the South Atlantic during the Jurassic-Cretaceous (Rossello et al., 2000). Despite the genetic link, the basins present distinct volcano-sedimentary infill and are separated by the NPT, where only smaller rift basins are found (Rossello et al., 2000). The SaLAM was formed during extensional tectonics related to Pangea breakup, with a later dextral transtensive phase associated by Rossello et al. (2000, 2007) with the drifting movement that led to the completion of South Atlantic opening. The Santa Lucia Basin corresponds to the SW part of the SaLAM, presents a central structural high with E-W strike and comprises mostly siliciclastic deposits, reaching a total thickness of 2.500 m (Rossello et al., 2000; Veroslavsky et al., 2004). The NE SaLAM is represented by the Laguna Merin Basin, which is mainly composed of volcanic rocks with ages between 134 and 127 Ma and covered by Cenozoic sedimentary rocks (Cernuschi et al., 2015).

3. Materials and methods

3.1. Sampling

For this study we collected basement samples from 32 outcrops across Uruguay (Fig. 2). We avoided locations with published low-temperature thermochronometry data and aimed to cover most of the shield, collecting samples from the margins and central parts of each tectonostratigraphic terrane. Standard crushing, magnetic and heavy liquids separation were processes applied to isolate the apatite and zircon crystals from the samples. Although we sampled mainly granitic rocks, which are usually rich in apatite and zircon, only 21 samples provided crystals suitable for the thermochronometry analysis (Fig. 2, Table 1).

3.2. Low-temperature thermochronometry

We used three low-temperature thermochronometers to investigate the thermal evolution of the Uruguayan basement: apatite fission-tracks (AFT), apatite (U−Th)/He (AHe) and zircon (U−Th)/He (ZHe). These radio-isotopic systems have distinct retention temperatures, under which the radioactive decay products are retained within the crystals, and together they cover an interval between *c.* 40 to 190 °C, simply put, shallow crust temperatures. Moreover, each method has a temperature interval where accumulation and loss of the radiogenic decay products compete, in which lower temperatures favor the accumulation of the decay products and higher temperatures their disappearance. Above such temperature interval, particular to each thermochronometer, the high temperatures cause the complete loss of the radiogenic products,

resetting the thermochronometer age to zero.

Apatite fission-tracks thermochronometry is based on the accumulation of linear defects (tracks) in the crystal lattice, formed by spontaneous fission of ^{238}U. The quantity and lengths of the tracks indicate the thermal path experienced by the crystal (Price and Walker, 1963; Fleischer et al., 1975; Gleadow et al., 1986a, 1986b; Galbraith et al., 1990). The apatite fission-track partial annealing zone (AFTPAZ) corresponds to temperatures between *c.* 60 to 110 °C, in which the tracks slowly shrink in a process known as annealing (Wagner et al., 1989). Below *c.* 60 °C the annealing process is not effective, and tracks are preserved with their full initial length (*c.* 16 μm). Although temperature is the main factor controlling annealing, this process is also affected by variations in apatite chemical composition and the amount of accumulated radiation damage (Gleadow et al., 1986a; Stockli, 2005; Tagami and O'Sullivan, 2005). Apatite fission track ages can be determined based on the density of spontaneous tracks in the crystal, formed because of ^{238}U decay, and of induced tracks, formed artificially in a nuclear reactor. The balance between spontaneous and induced tracks provides the uranium content and the age of the crystal. Furthermore, the distribution in the length of the spontaneous tracks and their mean value (MTL) indicate the cooling/heating events experienced by the hosting rock.

We used the external detector method for AFT dating (Gleadow, 1981; Hurford, 1990). For each sample, > 200 apatites were handpicked and mounted in epoxy resin tablets, polished to the central portion, and etched in a 5.5 M HNO3 solution at 21 °C for 20 s to reveal the spontaneous fission tracks (Carlson et al., 1999). Muscovite sheets were coupled to the tablets, which then were irradiated at the IEA-R1/IPEN-CNEN Reactor, São Paulo, Brazil, along with Durango age standards and Corning CN5 dosimeters. Afterwards, mica sheets were decoupled and etched in 48% HF for 18 min at 20 °C to reveal the induced tracks. AFT analyses were performed at the Universidade Federal do Rio Grande do Sul, Brazil, using a Leica DM 6000 M Microscope (1000×, dry). Ages were calculated based on 20 crystals per sample and the ζ calibration method (Hurford and Green, 1983; Hurford, 1990), while ages homogeneity was analyzed through the chi-square test (Galbraith, 1981; Galbraith and Green, 1990) using the software RadialPlotter 9.0 (Vermeesch, 2009). For thermal modeling we aimed to measure lengths and *c*-axis angles of 100 confined tracks in each sample, which allowed projection of the length of each track on this axis, as the annealing efficiency varies with respect to the crystallographic axes (Donelick et al., 1999). Furthermore, we used the mean etch pit diameter D_{par} from about 100 measurements as kinetic parameter, as it is a proxy for the crystal's chemical composition, which also affects the annealing efficiency (Donelick, 1993; Carlson et al., 1999; Donelick et al., 2005).

The (U−Th)/He method is based in the accumulation of alpha particles (^{4}He) in the crystal lattice after the decay chain of ^{238}U, ^{235}U and ^{232}Th isotopes. The alpha particles are expelled from the mineral structure at high temperatures owing to thermal diffusion. In apatite (U−Th)/He dating, alpha particles are efficiently expelled at temperatures above *c.* 70 °C, partially retained between *c.* 40 and 70 °C (AHe Partial Retention Zone – AHePRZ), and completely retained when temperature is below *c.* 40 °C (Wolf et al., 1996, 1998; Farley, 2002). However, these temperature limits are known to vary with crystal dimensions, compositional zonation, eU concentration (eU = [U] + 0.235 × [Th]) and accumulated radiation damage (Farley, 2000; Reiners and Farley, 2001; Shuster et al., 2006). Moreover, small fluctuations in these factors are magnified by extended residence in the AHePRZ, commonly resulting in dispersed AHe ages (Flowers and Kelley, 2011; Green and Duddy, 2018). In zircon (U−Th)/He dating, alpha particles are partially retained between *c.* 150 and 190 °C (ZHe Partial Retention Zone – ZHePRZ), and promptly expelled at temperatures higher than 200 °C (Reiners et al., 2018). Similarly to AHePRZ, the ZHePRZ is affected by compositional zonation, eU concentration, accumulated radiation damage and protracted residence at low temperatures (Reiners et al., 2002, 2004; Nasdala et al., 2004; Reiners, 2005).

The (U−Th)/He analyses were conducted in the Arizona Radiogenic Helium Dating Laboratory (ARHDL), at the University of Arizona, US. Both apatites and zircons were handpicked based on morphology, size and optical clarity, using a Leica MZ16 microscope. Preference was given to clear apatites with both terminations, aiming to avoid crystals that loss ^{4}He through fractures or a highly damaged crystal lattice. Similarly, unbroken zircons were selected but, since zircon eU usually is one or two orders of magnitude higher, we picked zircons with a wide range of opacity, which ultimately reflect the amount of accumulated radiation damage, and provide a better view of the eU influence over the ZHe age (Ault et al., 2018). Crystals were measured and photographed with Leica Application Suite V3, to define the diffusion domain and allow the alpha-ejection age correction (Farley et al., 1996), which accounts for the ejection of ^{4}He in crystal rims during decay. After Reiners (2005) analytical method, Nb foil tubes were used to pack the crystals for helium extraction, completed using long-wavelength laser heating and measured with a quadrupole mass spectrometer. Subsequently, crystals were dissolved in a HF-HNO_3 mixture for the U−Th measurements, performed using a high-resolution Element2 ICP-MS. Durango standards and blank samples were systematically introduced in between analysis to guarantee reliability of the measurements.

3.3. Inverse thermal modeling

The thermal history of each sample was recreated using the program QTQt 5.7, which tests time-temperature points aiming to reconstruct a thermal history that predicts and reproduces the observed thermochronometric data (Gallagher et al., 2009; Gallagher, 2012). We opted to run models with a minimum of user-imposed constraints, to avoid a biased thermal history. To initiate our models, a large t-T box was set with time ranging from 500 ± 50 Ma and temperature from 100 ± 100 °C, time corresponding to the end of the Brasiliano/Pan-African cycle (de Almeida et al., 1981; Hasui, 2010). A final constraint was set with temperature of 20 ± 10 °C at the present time. The thermal history between initial and final constraints was recreated freely by QTQt 5.7, using a temperature range of 70 ± 70 °C when modeling only AFT and AHe, and up to 100 ± 100 °C when ZHe data were available.

Because our current understanding of the AFT system is arguably better established than the (U−Th)/He system, trial models were run only with AFT data at first, and (U−Th)/He data were included in posterior models. Several fast runs of 20,000 interactions were made initially for each sample to set appropriate parameters during inversion (see Gallagher, 2012), and to test the variability of models using different $\partial T/\partial t$ rates. Models run only with AFT data resulted in good fit between observed and predicted ages and MTL, but the inclusion of AHe data into the models led to a considerable mismatch of the AFT data. The later models predicted older AFT ages than the observed while attempting (and usually failing) to fit all AHe ages without improving the low temperature (< 60 °C) thermal history. To address this conflict and maintain a good fit of our AFT data, we used a feature from QTQt 5.7 that resamples the AHe age error in order to accept a larger degree of mismatch of AHe data. This way the models were controlled mainly by the AFT data (ages and MTLs) and the sample's thermal path was not affected by significant distortions caused by the disperse AHe ages (see Sections 4.2 and 5.1, and the Supplementary material). On the other hand, the inclusion of ZHe data usually better constrained the cooling trajectory from higher temperatures (> 150 °C) in the models. Final models combined all thermochronometry data available for each sample, were run for 200,000 interactions or more, and used a maximum $\partial T/\partial t$ of 10 °C/Ma, compatible with a cratonic region of subdued topography. This final modeling set up allowed the proposed time-temperature paths to be well defined but not tightly limited by our constraints or by the old and dispersed AHe ages (see Results and Interpretations). During modeling, for AFT we used the D_{par} values and *c*-

Table 2
Apatite fission-track data from the Uruguayan shield. Ages were calculated using ζ = 280.17. N: number of grains analyzed; ρs: spontaneous track density; Ns: number of spontaneous tracks counted; ρi: induced track density; Ni: number of induced tracks counted; ρd: dosimeter tracks density; Nd: number of tracks used to determine ρd; χ^2: chi-square probability of single population; U: estimated value of uranium content; Dpar: mean etch pit diameter; CT: confined tracks measured; MTL: mean track length; SD: standard deviation of mean track length distribution; cP.MTL: c-axis projected mean track length; cP. SD: standard deviation of c-axis mean track length; (−): data not available.

Apatite Fission Tracks analysis																	
Sample	N	ρs	Ns	ρi	Ni	ρd	Nd	Central age	± 1σ	χ2	U	Dpar	CT	MTL	± 1σ	SD	*c*P. MTL	*c*P. SD
#	#	(x10^5)	#	(x10^5)	#	(x10^5)	#	(Ma)	(Ma)	(%)	(ppm)	(μm)	#	(μm)	(μm)	(μm)	(μm)	(μm)
Cuchilla Dionísio Terrane																		
UY2	20	18.91	779	10.46	431	7.17	14,341	179.0	10.8	88	18.5	1.87	100	11.46	0.15	1.48	13.31	0.90
UY29	20	9.16	338	4.12	152	7.17	14,341	219.6	21.5	99	7.3	1.79	100	10.18	0.22	2.22	12.31	1.39
UY30	20	12.96	359	12.85	356	7.00	13,999	98.1	7.4	69	23.3	2.18	100	12.57	0.18	1.83	13.89	1.43
UY31	20	15.5	369	10.76	256	7.17	14,341	143.2	11.7	94	19.1	2.04	100	12.73	0.16	1.63	13.93	1.31
UY32	20	15.14	542	13.85	496	7.17	14,341	108.3	8.1	11	24.5	1.91	100	12.71	0.17	1.65	14.08	1.07
Nico Pérez Terrane																		
UY1	20	19.25	460	9.92	237	7.17	14,341	192.1	15.4	99	17.6	1.82	100	11.17	0.12	1.21	13.00	0.80
UY6	20	12.29	515	5.25	220	7.17	14,341	230.9	18.7	95	9.3	1.88	100	11.52	0.14	1.44	13.31	0.88
UY7	20	17.97	532	9.19	272	7.00	13,999	189.0	14.2	98	16.7	1.81	100	11.53	0.12	1.25	13.24	0.84
UY8	20	13.24	507	7.60	291	7.17	14,341	172.7	12.8	99	13.5	1.90	100	11.56	0.13	1.34	13.30	0.83
UY10	20	4.06	204	3.17	159	7.00	13,999	125.4	14.1	59	5.7	1.87	–	–	–	–	–	–
UY11	20	5.3	114	4.84	104	7.17	14,341	109.2	14.8	100	8.6	1.79	30	12.68	0.29	1.61	13.87	1.23
UY14	20	3.47	191	4.05	223	7.17	14,341	85.8	8.4	100	7.2	1.88	52	12.23	0.21	1.53	13.72	1.16
UY21	20	8.39	308	5.42	199	7.17	14,341	153.6	14.0	94	9.6	1.87	42	12.43	0.23	1.49	13.84	1.04
Piedra Alta Terrane																		
UY16	20	10.71	422	5.38	212	7.00	13,999	192.3	16.3	100	9.8	1.76	100	12.00	0.15	1.45	13.58	0.99
UY25	20	18.78	417	8.06	179	7.17	14,341	229.9	20.6	82	14.3	1.99	100	12.05	0.14	1.45	13.54	1.10
UY26	20	22.09	612	10.87	301	7.17	14,341	201.1	14.3	74	19.2	2.27	100	12.20	0.14	1.38	13.73	0.87
UY27	20	12.69	387	6.59	201	7.00	13,999	186.1	16.2	99	12.0	2.03	100	11.50	0.15	1.46	13.18	1.04
Tadilia Terrane																		
UY18	20	13	360	7.94	220	7.00	13,999	158.5	13.6	100	14.4	1.77	100	11.59	0.15	1.47	13.30	0.95
UY19	20	13.79	222	9.63	155	7.17	14,341	144.0	16.2	53	17.1	1.86	38	11.25	0.29	1.78	13.08	1.11

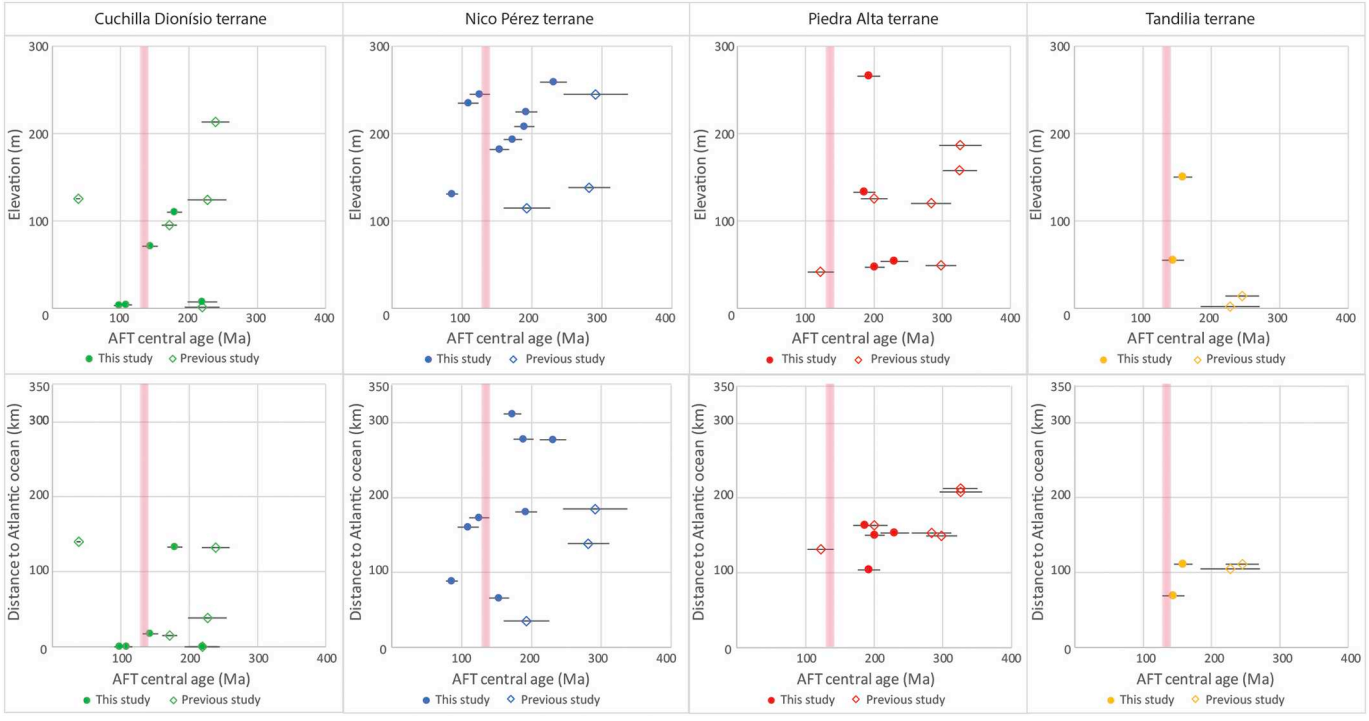

Fig. 3. Compilation of AFT data available for the Uruguayan shield (this work; Kollenz, 2015; Gomes and Almeida, 2019). Top row shows plots of AFT central ages against elevation, with a tendency of positive correlation for the CDT, NPT and PAT. Bottom row shows AFT ages against the shortest distance to the Atlantic margin in the east, with positive correlation for the NPT and PAT as well. Vertical red bar indicates the Paraná-Etendeka LIP volcanism. (For interpretation of the references to colour in this figure legend, the reader is referred to the web version of this article.)

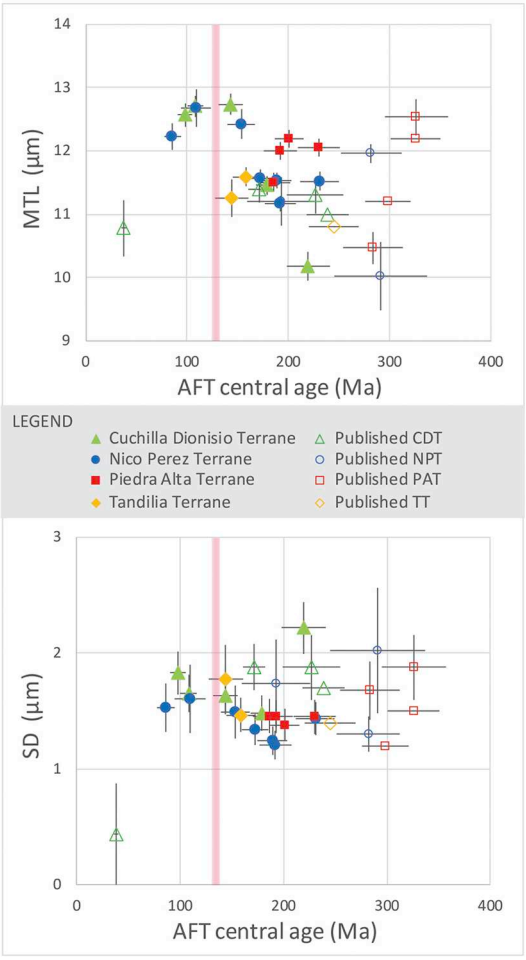

Fig. 4. Compilation of AFT data available for the Uruguayan shield. In the top, AFT central ages against MTLs uncorrected for their c-axis orientation, suggesting that samples went through protracted cooling without partial resetting during the Paraná-Etendeka LIP volcanism (vertical red bar), and with distinct parts of the shield cooling below 110 °C at different times. In the bottom, plot of the AFT central ages against the standard deviation of the MTLs, which also does not show a "boomerang" shape. Error bars represent ± 1σ range. (For interpretation of the references to colour in this figure legend, the reader is referred to the web version of this article.)

axis projected tracks lengths (Donelick, 1993; Donelick et al., 1999), the AFT annealing model from Ketcham et al. (2007), and the radiation damage model from Flowers et al. (2009) for AHe and from Guenthner et al. (2013) for ZHe.

4. Results and interpretations

The results from each thermochronometer and from the inverse modeling are outlined in the subsections below. General interpretations are briefly commented as well, however the particularities of the results inserted in the geological context on Uruguay are explored in the Discussion and integration section.

4.1. Apatite Fission-tracks

We obtained AFT ages from 19 samples (Table 2), all of which passed the homogeneity chi-square test ($P\chi^2 > 5\%$) and generally did not show single grain age dispersion, which means that the central ages obtained correspond to single populations. Three samples presented minor age dispersion (UY10 = 17%, UY19 = 18% and UY32 = 18%) that could indicate a mix of apatite populations, but because they passed the chi-square test and their central ages agree with neighborhood samples, we considered them as single population also (see Supplementary material). All obtained ages are Mesozoic, ranging from 230.9 ± 18.7 Ma to 85.8 ± 8.4 Ma (Late Triassic to Late Cretaceous), with the majority situated in the Jurassic Period. In general, the younger ages are near the coast or structural lineaments, while the older ones are hinterland (Fig. 2), in a common distribution of ages of passive margins (Gallagher and Brown, 1997). When including data from previous AFT studies in the region (Kollenz, 2015; Gomes and Almeida, 2019), a weak to moderate positive correlation between ages and elevation or distance to the Atlantic Ocean is suggested (Fig. 3). The NPT presented simultaneously one of the oldest AFT age in our set (sample UY6 with *c.* 230 Ma, located in the north on the Isla Cristalina de Rivera) and also the youngest AFT age (UY14 with *c.* 85 Ma, in the southern-central portion of the terrane). This deviation can be related to the complexity of the NPT, composed of distinct rock associations and cut by several faults and shear zones, prone to variable exhumation within the terrane. Sample UY14 for example, the youngest one, is located near a major fault, and might reflect the last stage of tectonic reactivation of this structure at the time of Campanian rhyolitic volcanism (Gaucher et al., 2016).

The non-projected mean track lengths (MTL) of all samples are rather medium to short, ranging from 12.7 ± 0.2 to 10.2 ± 0.2 µm (Table 2). After applying the *c*-axis projection (Donelick et al., 1999), the MTL range from 13.9 to 12.3 µm, with standard deviation between 1.4 and 0.8 µm. The lengths scattering tends to be unimodal for all samples but UY29, which displays a bimodal distribution and a distinct old AFT age in the SSE coastal region (CDT). In most cases, the track lengths distribution is Gaussian around the mean value or negatively skewed, with a larger proportion of longer tracks (see Supplementary material), which can be interpreted in terms of protracted cooling (Gallagher and Brown, 1999). A plot of the MTLs against AFT central ages (Fig. 4), including published data (Kollenz, 2015; Gomes and Almeida, 2019), does not show a clear "boomerang" shape (Green, 1986), which is characteristic of reheating with partial reset of AFT ages in a region. Instead it suggests that samples went through protracted cooling without a major reheating, and with distinct parts of the shield cooling below 110 °C at different times. Measurements of the D_{par} range between 2.27 and 1.76 µm, which indicates a predominance of chlorine rich apatites, with high resistance to annealing (Carlson et al., 1999; Donelick et al., 2005).

4.2. Apatite (U−Th)/He

Apatites from 14 locations were selected for AHe analysis, in total representing 42 single crystal ages (Table 3). The obtained ages present are widely dispersed, not only between samples and terranes, but also among apatites from each sample, in a similar way as observed by Hueck et al. (2017). The AHe uncorrected ages range throughout the Phanerozoic, but the majority of them are Mesozoic. No reduction in the age dispersion is observed after applying the Ft correction (Farley et al., 1996). Furthermore, the AHe ages obtained are mostly older than the AFT ages from the same location, portraying an inverse pattern that is often observed in cratonic regions and likely related to the accumulation of radiation damage within the crystals and protracted residence at temperatures inside the AHePRZ (see Section 5.1) (Flowers and Kelley, 2011).

A common approach to investigate AHe ages dispersion is to evaluate the influence of the crystal radius and integrity (if broken or not) (Reiners and Farley, 2001; Brown et al., 2013), and of the effective uranium (eU) content of crystals (Flowers et al., 2007), factors that commonly affect AHe ages. In general, our samples do not show a clear correlation between ages and these parameters, suggesting that other factors are responsible for the AHe ages dispersion. Several variables can influence AHe ages, including U and Th zonation (Farley et al., 1996; Flowers and Kelley, 2011), U-rich inclusions (Stockli et al.,

Table 3
Summary of Apatite (U–Th)/He ages and parameters. Crystal dimensions were used to estimate an equivalent spherical radius. eU, total uranium content; Term, number of crystal terminations; Unc., uncorrected; Corr., corrected; SD, standard deviation; Ft, alpha ejection factor for age correction.

Apatite (U–Th)/He analysis																		
Sample	Crystal	U	Th	Sm	He	eU	Term.	Radius	Age unc.	± 1σ	Ave. unc.	SD	± 1σ	Ft	Age corr.	± 1σ	Ave. corr.	SD	± 1σ
#	#	(ppm)	(ppm)	(ppm)	(nmol/g)	(ppm)	#	(μm)	(Ma)	(Ma)	(Ma)	(Ma)	(Ma)	#	(Ma)	(Ma)	(Ma)	(Ma)	(Ma)
Cuchilla Dionísio Terrane																			
UY2	1	59.92	130.15	488.89	146.82	92.67	1	57.38	292.10	5.96	441.09	106.69	61.60	0.74	392.38	8.07	546.46	109.62	63.29
	2	21.79	61.86	368.63	101.75	37.99	1	79.51	494.97	10.11				0.81	608.67	12.54			
	3	8.78	24.84	305.88	45.05	16.03	2	92.53	536.20	11.07				0.84	638.33	13.27			
UY30	1	8.13	12.82	214.17	7.49	12.14	2	42.71	120.51	2.68	107.98	10.71	6.18	0.67	180.31	4.03	152.31	21.71	12.53
	2	24.29	19.84	478.29	15.14	31.18	2	55.35	94.34	1.31				0.74	127.41	1.77			
	3	9.85	8.15	18.56	7.00	11.85	1	53.89	109.09	1.69				0.73	149.21	2.33			
UY32	1	59.86	11.48	467.66	38.88	64.74	2	40.45	113.17	2.51	135.58	50.08	28.91	0.66	171.81	3.83	196.36	69.34	40.03
	2	45.55	5.08	421.35	22.73	48.72	1	46.78	88.60	1.97				0.70	126.41	2.83			
	3	46.53	4.36	447.24	54.10	49.65	1	46.86	204.97	4.58				0.70	290.85	6.54			
UY24	1	3.91	2.21	271.49	4.03	5.70	1	45.94	155.03	4.61	211.19	56.16	39.71	0.71	219.65	6.55	314.97	95.32	67.40
	2	2.22	1.89	469.70	4.75	4.87	1	34.84	267.35	10.79				0.65	410.29	16.33			
Nico Pérez Terrane																			
UY1	3	14.64	2.24	157.52	8.04	15.90	1	62.41	96.34	2.15	131.16	29.66	17.13	0.77	125.01	2.80	170.41	32.60	18.82
	4	19.69	54.24	222.63	22.89	33.42	1	47.23	128.32	1.81				0.69	186.17	2.65			
	5	26.26	25.87	124.55	30.01	32.90	2	95.87	168.83	2.52				0.84	200.06	3.00			
UY6	1	7.99	36.96	66.71	15.38	16.96	2	66.62	167.83	3.39	262.62	67.12	38.75	0.77	218.10	4.42	346.05	90.48	52.24
	2	9.03	43.73	74.69	32.68	19.61	2	59.49	305.66	6.20				0.75	409.89	8.37			
	3	5.90	24.48	68.68	20.36	11.95	2	64.67	314.37	6.41				0.77	410.17	8.42			
UY8	1	4.54	15.55	44.52	7.53	8.39	1	47.93	166.91	2.27	182.64	40.46	18.09	0.69	241.31	3.32	281.44	63.42	28.36
	2	21.50	41.04	72.27	21.49	31.45	2	38.08	126.17	1.46				0.63	201.46	2.37			
	3	11.28	50.36	358.19	30.32	24.75	2	41.09	234.61	3.28				0.65	362.35	5.08			
	4	11.46	44.23	88.01	24.41	22.22	1	39.51	202.88	2.86				0.63	320.65	4.56			
UY11	1	4.25	36.85	694.43	20.01	16.14	2	52.86	265.25	3.24	208.62	48.20	27.83	0.72	367.60	4.44	285.99	61.74	35.65
	2	6.21	43.76	359.92	13.63	18.14	1	45.83	147.43	1.89				0.68	218.29	2.79			
	3	8.34	74.17	621.66	30.96	28.61	1	71.44	213.17	2.59				0.78	272.07	3.29			
UY14	1	3.10	23.24	96.80	4.47	9.00	2	73.47	94.61	1.22	103.01	16.33	7.30	0.79	120.26	1.55	133.43	20.82	9.31
	2	3.92	24.81	91.44	6.31	10.16	2	62.63	117.32	1.33				0.75	155.65	1.76			
	3	5.86	22.81	69.82	4.94	11.53	2	62.61	80.37	0.90				0.76	106.26	1.19			
	5	2.84	20.74	85.27	5.10	8.09	2	74.51	119.73	1.42				0.79	151.57	1.79			
UY21	1	18.58	52.98	716.38	15.92	97.71	1	41.89	91.78	1.90	105.94	14.16	8.18	0.68	139.63	2.90	152.94	13.31	7.69
	3	9.90	20.42	218.52	9.79	16.23	2	52.63	120.10	2.57				0.71	166.25	3.58			
Piedra Alta Terrane																			
UY16	1	6.08	24.39	164.32	14.82	12.56	2	54.18	224.94	2.63	250.26	18.01	10.40	0.73	310.02	3.64	328.44	23.04	13.30
	2	8.40	23.61	171.26	20.68	14.73	2	55.50	265.35	2.98				0.74	360.93	4.09			
	3	10.39	8.93	103.22	18.10	12.96	2	85.64	260.49	3.26				0.83	314.37	3.96			
UY25	1	56.87	38.42	271.62	64.15	67.13	1	49.97	176.95	3.78	258.83	59.84	34.55	0.72	247.45	5.32	368.18	85.42	49.32
	2	25.50	24.77	219.10	55.67	32.33	1	56.98	318.28	6.78				0.75	424.81	9.15			
	3	27.21	24.40	212.86	51.57	33.92	2	39.58	281.27	6.07				0.65	432.29	9.47			
UY27	1	13.43	16.16	314.13	30.29	18.69	2	46.35	311.03	3.97	263.80	34.10	19.69	0.70	445.54	5.76	388.25	40.51	23.39
	2	23.25	42.01	431.60	42.83	35.11	2	39.54	231.74	2.76				0.64	359.42	4.34			
	3	19.50	36.16	468.71	39.06	30.16	2	46.06	248.63	2.92				0.69	359.80	4.27			
Tandilia Terrane																			
UY18	1	9.44	2.74	129.44	12.50	10.69	2	49.67	222.16	6.50	201.68	21.16	10.58	0.72	308.79	9.10	289.96	34.86	17.43
	2	16.26	12.18	136.90	18.21	19.75	2	50.06	172.54	3.98				0.72	241.10	5.60			
	3	12.28	4.32	108.17	15.50	13.79	2	40.05	210.33	5.11				0.66	320.01	7.86			

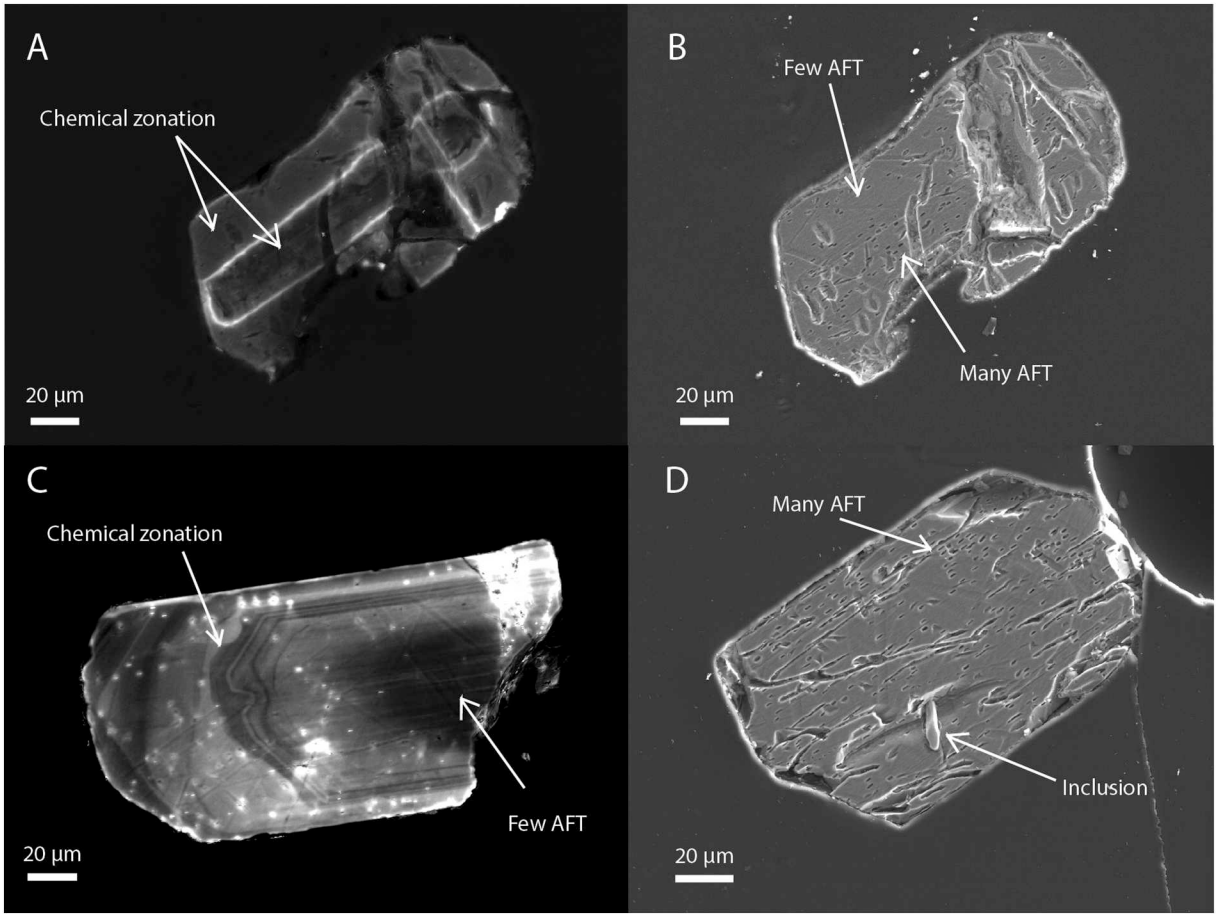

Fig. 5. Photomicrographs of apatites showing factors that can affect the (U-Th/He) analysis and cause significant age inaccuracies. (A,B) Cathodoluminescence and secondary electron images from the same apatite from UY32 showing a brightly marked chemical zonation coincident with a fission-track density zonation. (C) Cathodoluminescence from apatite from UY8 showing chemical zonation and a low density of tracks in the center. (D) Secondary electron image from apatite from UY27 showing inclusion and a higher density of tracks in the rims.

2000), ^{4}He implantation from U-rich neighbor minerals and phases (Murray et al., 2014), accumulated radiation damage on the crystal lattice (Green and Duddy, 2006; Shuster et al., 2006), among others – see Wildman et al. (2016) for a summary of the influence of these and others factors. These variables can be responsible for the ages dispersion, as in sample UY2, collected from a region of eU rich granites and that present old AHe ages and high values of ^{4}He for its eU content, making ^{4}He implantation or U-rich inclusions likely occurrences. At the same time, Fig. 5 shows apatites from samples UY8, UY27 and UY32 that were subjected of AFT analysis and exhibits chemical zonation and inclusions. Although the images are not from crystals used for AHe dating, they represent common features in these samples that potentially affected our AHe ages. The presence of inclusions, zonation or defects in the crystal lattice can lead to highly dispersed ages and mask the common correlations between ages and eU or crystal radius. However, because dispersion is observed in most of our samples, a more general approach is desired to explain our AHe results, as suggested in the Discussion and integration section. Moreover, we opted to report in Fig. 2 the youngest AHe age for each location, which potentially represents the age least affected by factors such as implantation and inclusions, and would be closer to the actual cooling age of the sample and correspond to the standard closure temperature (Dodson, 1973) of the AHe system. Meanwhile, all AHe ages for each location, dispersion and further data are displayed in Table 3.

4.3. Zircon (U−Th)/He

A total of 40 zircons were dated from eight locations across the UYS (Table 4). Single crystal ZHe ages range through the entire Paleozoic and show a strong negative correlation with eU, unlike our AHe ages (Fig. 6). Such negative correlation is common in cratonic regions and usually is attributed to long-term accumulation of radiation damage in the crystals. Zircons with high eU and long low-temperature histories are prone to develop a damage net within the crystalline lattice, which increases the diffusivity and loss of alpha particles, thus resulting in younger ages (Reiners, 2005; Guenthner et al., 2013). Considering this, we opted to show in the map (Fig. 2) the oldest single grain ZHe age for each location, usually Cambrian/Ordovician for the NPT and CDT samples, and Permian for the PAT. The oldest ZHe age potentially represents the cooling age of the least damaged zircon analyzed, likely closer to the beginning of the ^{4}He accumulation within the sample and to the standard closure temperature of the ZHe system. The complete dataset of the ZHe analysis is shown on Table 4. No correlation between ZHe ages and crystal radius, location or altitude was observed in our samples.

Table 4
Summary of Zircon (U−Th)/He ages and parameters. Crystal dimensions were used to estimate an equivalent spherical radius. eU, total uranium content; Unc., uncorrected; Corr., corrected; SD, standard deviation; Ft, alpha ejection factor for age correction.

Zircon (U−Th)/He analysis																	
Sample	Crystal	U	Th	He	eU	Radius	Age unc.	± 1σ	Ave. unc.	SD	± 1σ	Ft	Age corr	± 1σ	Ave. corr.	SD	± 1σ
#	#	(ppm)	(ppm)	(nmol/g)	(ppm)	(μm)	(Ma)	(Ma)	(Ma)	(Ma)	(Ma)	#	(Ma)	(Ma)	(Ma)	(Ma)	(Ma)
Cuchilla Dionísio Terrane																	
UY2	1	1216.02	636.19	1592.79	1365.52	36.94	212.40	3.02	273.11	68.31	30.55	0.68	311.46	4.49	371.45	86.13	38.52
	2	773.03	215.67	1214.88	823.71	39.61	267.17	5.04				0.70	379.04	7.24			
	3	741.36	175.63	1292.37	782.64	52.87	298.24	5.68				0.77	385.10	7.41			
	4	395.44	195.09	957.90	441.28	47.41	389.04	7.28				0.75	518.30	9.84			
	7	1267.26	388.53	1480.69	1358.56	48.81	198.68	3.71				0.75	263.37	4.96			
UY29	1	543.50	270.19	1130.77	606.99	61.94	335.50	4.39	299.50	80.16	35.85	0.80	417.01	5.52	395.12	94.15	42.11
	2	293.29	213.03	693.26	343.35	50.85	362.95	4.57				0.76	475.00	6.09			
	3	1963.03	622.64	2228.84	2109.35	42.73	192.73	2.84				0.72	266.84	3.97			
	4	298.36	167.44	736.46	337.71	50.99	390.86	5.61				0.77	509.99	7.43			
	5	704.82	281.30	912.64	770.93	39.63	215.49	3.13				0.70	306.73	4.52			
UY32	1	2844.44	1344.08	1280.10	3160.30	94.20	74.66	1.03	121.47	29.46	13.18	0.87	86.22	1.20	152.75	40.98	18.33
	2	1943.91	245.54	1307.62	2001.62	59.78	119.95	1.73				0.80	150.63	2.18			
	3	1857.49	725.71	1768.94	2028.03	57.63	159.57	2.22				0.79	202.44	2.83			
	4	1138.28	3274.83	1505.60	1907.87	55.28	144.52	1.60				0.77	187.89	2.09			
	5	1542.94	344.60	960.09	1623.92	59.83	108.67	1.50				0.80	136.58	1.90			
Nico Pérez Terrane																	
UY8	1	438.83	158.79	1033.20	476.15	77.94	388.74	6.15	377.98	21.07	9.42	0.84	460.49	7.35	456.99	16.15	7.22
	2	281.82	94.67	569.75	304.06	55.21	337.27	5.32				0.78	430.51	6.87			
	3	280.84	77.47	647.22	299.04	88.50	387.67	6.27				0.86	449.53	7.32			
	4	350.88	76.05	817.60	368.75	70.52	396.72	5.74				0.83	478.21	6.98			
	5	281.90	113.49	653.05	308.57	64.82	379.52	5.32				0.81	466.22	6.61			
UY10	2	1519.54	1104.20	1203.76	1779.03	32.76	124.16	1.53	213.19	89.58	40.06	0.64	193.48	2.43	297.42	109.43	48.94
	3	1821.40	1769.65	1672.24	2237.27	37.42	137.00	1.65				0.68	201.41	2.47			
	4	758.05	703.75	812.20	923.43	39.14	160.89	1.98				0.69	231.92	2.90			
	6	415.63	219.89	836.49	467.30	43.53	322.77	5.21				0.73	443.12	7.25			
	7	489.04	235.10	969.29	544.29	52.03	321.12	5.19				0.77	417.14	6.82			
UY13	1	646.57	326.51	1441.94	723.30	54.84	358.30	6.20	365.08	12.08	5.40	0.78	458.57	8.03	469.36	8.45	3.78
	2	628.19	257.97	1467.16	688.81	60.34	381.89	6.69				0.80	476.73	8.45			
	3	491.98	235.19	1140.75	547.25	54.63	374.08	6.54				0.78	478.93	8.48			
	4	770.65	247.05	1600.27	828.70	44.30	347.24	5.86				0.73	472.45	8.09			
	5	560.25	224.84	1242.32	613.09	57.29	363.90	6.07				0.79	460.11	7.76			
Piedra Alta Terrane																	
UY27	1	851.37	116.24	755.00	878.69	90.84	157.22	2.19	170.76	40.11	17.94	0.86	182.07	2.54	206.24	46.65	20.86
	2	1102.95	316.03	1163.28	1177.22	60.71	180.43	2.46				0.80	225.73	3.10			
	3	1629.90	301.28	945.84	1700.71	60.34	102.28	1.44				0.80	128.27	1.81			
	4	483.89	69.39	525.97	500.19	68.89	191.79	3.14				0.82	233.07	3.84			
	5	670.02	204.32	876.64	718.04	80.79	222.08	3.49				0.85	262.08	4.14			
Tandilia Terrane																	
UY18	1	2012.46	328.91	1106.92	2089.76	59.72	97.46	1.61	154.81	42.01	18.79	0.80	122.52	2.03	207.89	59.07	26.42
	2	1670.14	299.44	1299.07	1740.51	47.60	136.83	1.86				0.75	182.88	2.51			
	4	1771.17	383.20	1365.69	1861.22	43.11	134.55	1.81				0.72	185.87	2.52			
	5	1105.25	334.62	1245.33	1183.88	44.39	191.87	2.58				0.73	262.18	3.56			
	6	784.68	167.61	965.85	824.07	46.85	213.35	3.77				0.75	286.00	5.10			

4.4. Inverse modeling

The thermal history of 19 locations was computed by inverse modeling and the results can be divided into two main groups with distinct cooling patterns. All models use AFT data as baseline, the thermochronometer with the most consistent regional results, but most of the models include (U−Th)/He data as well (see Supplementary material). Moreover, the physical proprieties of the AFT system (*e.g.* annealing rate variability caused by apatite chemical composition) are better understood in the scientific community if compared to the (U−Th)/He system (*e.g.* effects on ages caused by long residence in the partial retention zone), thus models based on AFT are arguable more robust (*e.g.* Green et al., 2006; Flowers and Kelley 2011; Green and Duddy, 2006, 2018; Weisberg et al., 2018). Final models display a good fit between observed and predicted AFT ages and MTL, a good fit of ZHe ages and usually a poor fit of AHe ages. Representative models are shown in Fig. 7 and the final models of each sample can be found in the Supplementary material.

Group 1 is composed of samples UY1, UY2, UY6, UY7, UY8, UY16, UY18, UY25, UY26 and UY27, located essentially in the west and NW of the shield (PAT, TT and northern part of the NPT). Models from these samples show passage through the AFTPAZ between *c.* 300 and 180 Ma (Fig. 8), with cooling rates varying between 0.60 and 0.32 °C/Ma. In most cases, entrance in the AFTPAZ (*c.* 110 °C) occurs in the Carboniferous-Permian transition, while cooling out from the zone (*c.* 60 °C) occurs by Late Triassic-Early Jurassic. Samples UY18 and UY27, which present relatively high eU content and young ZHe ages, went through the AFTPAZ slightly later and faster (*c.* 0.90 °C/Ma) than the general trend. The relatively high temperatures modeled for these two samples in the late Paleozoic might be caused by the accumulated radiation damage within the zircons, which eU tend to exceed 1000 ppm and can lower the closure temperature of the system (*e.g.* Hueck et al., 2018a). Similar behavior is observed in samples UY32 and UY10 from Group 2 (Fig. 9). Models from Group 1 suggest that in Early Cretaceous all these samples might have reached surface temperatures, which is supported by the AFT and AHe ages older than the Cretaceous magmatism, even

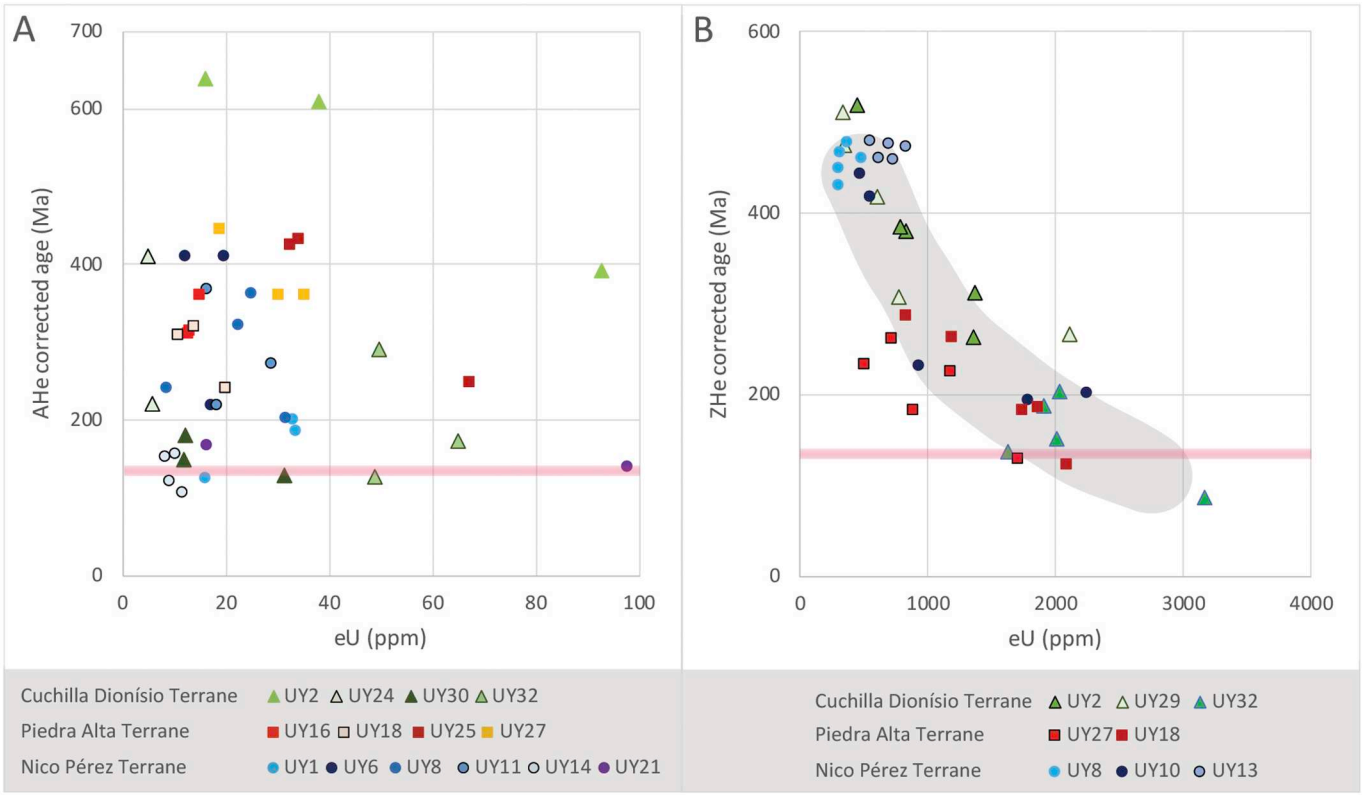

Fig. 6. Plots of (U-Th/He) corrected ages against effective uranium content (eU = [U] + 0.235 × [Th]). (A) AHe ages showing variable intrasample behavior and no apparent general trend. (B) ZHe ages clustered or showing a negative correlation intrasample. If all zircons are considered, a negative correlation between ages and eU is observed. Horizontal bar indicates the Paraná-Etendeka LIP volcanism.

though the thermal path is not well defined in the models during this epoch (Fig. 7). Afterwards, all models support a subtle reheating phase, that possibly lasted until the end of the Paleogene and raised temperatures slightly over 60 °C in some samples. This reheating is at the limit of the AFT method resolution, and possibly a modeling artifact (Jonckheere, 2003), a reflection of the considerably short length of the confined tracks of these samples, usually below 12 μm, which would require a prolonged time in the AFTPAZ. A final cooling towards surface temperature takes place by the Miocene. Sample UY29 resulted in a thermal history similar to Group 1 but with earlier and faster passage through the AFTPAZ, at a rate of 0.88 °C/Ma. Cooling into the AFTPAZ occurs by the Devonian-Carboniferous transition with an exit by the Permian. The model from this sample shows stability at temperatures around 30 to 50 °C until the Cretaceous, when a reheating phase occurred raising the temperature to 75 °C. A final cooling towards surface conditions is observed after the Paleocene. Sample UY29 is located in the extreme SE of the shield, where most samples present thermal histories belonging to Group 2.

Group 2 is composed of samples UY10, UY11, UY14, UY19, UY21, UY30, UY31 and UY32. These samples are located mostly in the center and SE of the shield (NPT and CDT), and are often near shear zones. Unlike Group 1, the models for these samples lack a Late Cretaceous reheating phase, and show a monotonic cooling towards surface since early Mesozoic. The time of cooling into the AFTPAZ occurs later than Group 1 and is variable among the samples, ranging between the Permian and Jurassic. Cooling occurs at rates between 0.30 and 0.71 °C/Ma, and during the Cretaceous all samples reached temperatures below 60 °C. Although Group 2 corresponds to protracted and monotonic thermal histories, it should be considered that these samples have a limited number (< 50) of confined tracks to be used during modeling, thus their models are less robust, except for sample UY30, UY31 and UY32, with 100 confined tracks each. Nonetheless, all of them have younger AFT ages and higher track length values (MTL) than Group 1, with lengths usually above 12.2 μm, even when 100 confined tracks were measured. Therefore, these monotonic thermal histories can represent Mesozoic tectonic activity in faults/shear zones or at the margins of the shield, especially near the Atlantic Ocean, but can also reflect their long and often limited number of confined tracks, which do not require a protracted period in the AFTPAZ or a reheating phase to shorten them as in Group 1.

5. Discussion and integration

In this study we combined three thermochronometers to investigate the cooling history of the Uruguayan shield. We presented a new dataset with 19 AFT, 42 AHe and 40 ZHe ages, plus the inverse thermal histories modeled for 19 locations. This dataset, combined with information from previous works (Kollenz, 2015; Hueck et al., 2017; Gomes and Almeida, 2019) provides an extensive coverage of the low-temperature history of the UYS. Based on the integration of these data, we characterized the thermal evolution of the shield during the Phanerozoic and discuss the exhumation of the basement, taking into account the apparent disparities between previous models.

5.1. Thermochronometry ages

All AFT ages obtained in this work are much younger than the host rock stratigraphic age and the last orogenic cycle that affected the region (Gondwana assembly during the Brasiliano/Pan-African cycle, late Neoproterozoic-Cambrian). Thus, we interpret our AFT ages as cooling ages that represent exhumation of the basement due to denudational events. There is good agreement between our AFT ages and those obtained by Kollenz (2015) and Gomes and Almeida (2019), totaling a combined dataset of 36 AFT ages across the UYS. While Kollenz (2015)

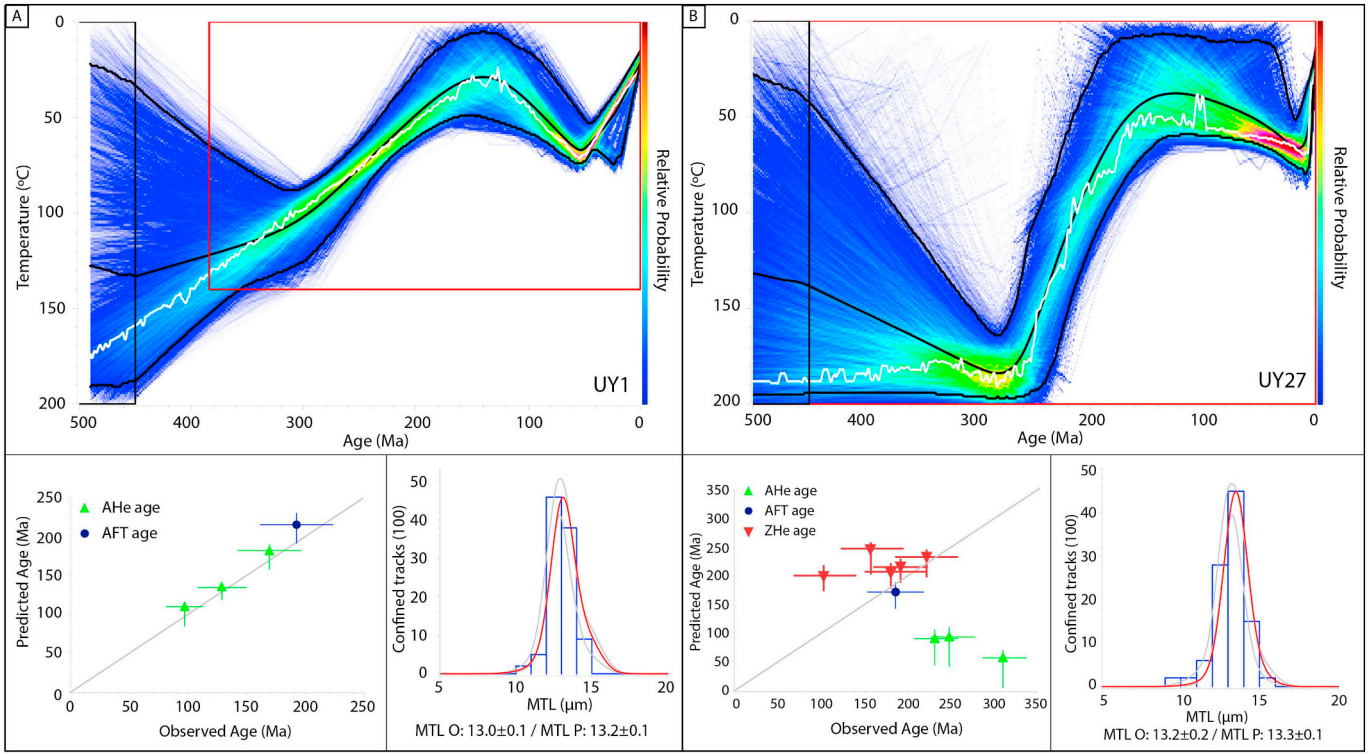

Fig. 7. Panel of representative inverse thermal models from Group 1. (A) On the top: Model for sample UY1. Black line represents the mean cooling trajectory, white line the maximum mode and colored pathway the 95% confidence interval with relative probability scale. Black rectangle is the start constraint box for the model, red box the prior to test thermal paths (see Gallagher, 2012). Bottom left: fit between observed ages and predicted ages by the model, including ± 1σ range. Bottom right: track length distribution with values of MTL observed and predicted by the model. (B): Same as in (A) but for sample UY27, with ZHe data. Misfit of AHe ages can be caused by the accumulation of radiation damage within the apatites (see Sections 3.3, 4.2 and 5.1 for more information). (For interpretation of the references to colour in this figure legend, the reader is referred to the web version of this article.)

obtained mainly Triassic (up to Permian) AFT ages on the western part of the UYS, Gomes and Almeida (2019) ages range essentially from the Permian to the Early Cretaceous and cover the four terranes of the UYS. Although the shield does not have significant topographic variations, a plot of the AFT central ages against sample elevation, including the works aforementioned, suggests positive correlations for the CDT, NPT and PAT (Fig. 3). Ages also tend to increase with the distance from the South Atlantic Ocean, a common pattern observed in continental passive margins (Gallagher and Brown, 1997). The PAT, representative of the Rio de La Plata Craton, and the northern part of the NPT, arguably part of the craton as well, concentrates the older AFT ages in Uruguay. Regarding the MTL, this work and those of Kollenz (2015) and Gomes and Almeida (2019) show remarkable similarities, both in the distribution (unimodal) and on the short to medium values (between 10 and 12.7 µm) of the track lengths, independently of the location in the shield. This pattern of tracks with reduced lengths implies that the samples went through a length residence in the AFTPAZ, allowing continuous annealing of the tracks. The medium-high D_{par} values of our samples, indicative of fairly high resistance to annealing (Carlson et al., 1999; Donelick et al., 2005), reinforce this interpretation.

Regarding the (U-Th/He) data, our AHe ages tend to be slightly older and present higher dispersion when compared to those obtained by Hueck et al. (2017), who reported mainly Permian to mid-Cretaceous ages after discarding crystals considered to be outliers. The wide dispersion of AHe ages within a sample can be attributed to internal factors, for example chemical zonation or ^{4}He implantation, that affect single aliquots (see Section 4.2). Moreover, although the AHe represents a lower temperature thermochronometer than the AFT system, our AHe ages are usually older than AFT ages from the same sample, in an inverse pattern common in cratonic regions (Flowers and Kelley, 2011). This inverted behavior is characteristic for apatite crystals with eU > 15 ppm subject to prolonged residence at temperatures below 70 °C, and augmented by reheating episodes that do not reset the AHe ages (Shuster et al., 2006; Reiners et al., 2018). Regardless, because inversion of AHe and AFT ages is a pattern in our dataset, and considerable dispersion of AHe ages is observed in almost every sample, these behaviors must be attributed to a more systematic mechanism. Considering that our samples are of Precambrian rocks, and that our models and AFT data indicate residence at low temperatures (< 110 °C) since the middle Mesozoic, it is likely that the analyzed apatites have accumulated a relatively high degree of radiation in the last 200 Ma. The damaged crystal lattice affects the diffusivity of the alpha particles within the apatites, initially increasing the retentivity of He, and resulting in abnormally old ages for the AHe system (Green and Duddy, 2006; Shuster et al., 2006). Furthermore, Shuster et al. (2006) claims that apatite with variable eU content and subject to a reheating episode after significant accumulation of radiation damage might present a large span of AHe ages, especially if the reheating increase temperatures to near 60 °C. Fox and Shuster (2014) demonstrate that apatites with different eU develop different retentivity of ^{4}He in a reheating event, and that minimal changes in the peak temperature during reheating cause large differences in the AHe ages and their eU correlation. Therefore, it is likely that some of our AHe ages are affected by intrasample factors, but it is plausible that the general behavior observed in the UYS is a consequence of accumulation of radiation damage in the apatites since the early Mesozoic. Moreover, the dispersion was likely augmented by an episode of subtle reheat in the region, which led to the broad range of AHe ages observed, accordingly to the sensitivity to the temperature peak of each individual crystal analyzed.

The accumulation of radiation damage plays a major role in our ZHe ages as well. If the density of damage sites overcome a threshold, they can become interconnected and decrease the retentivity of He, resulting

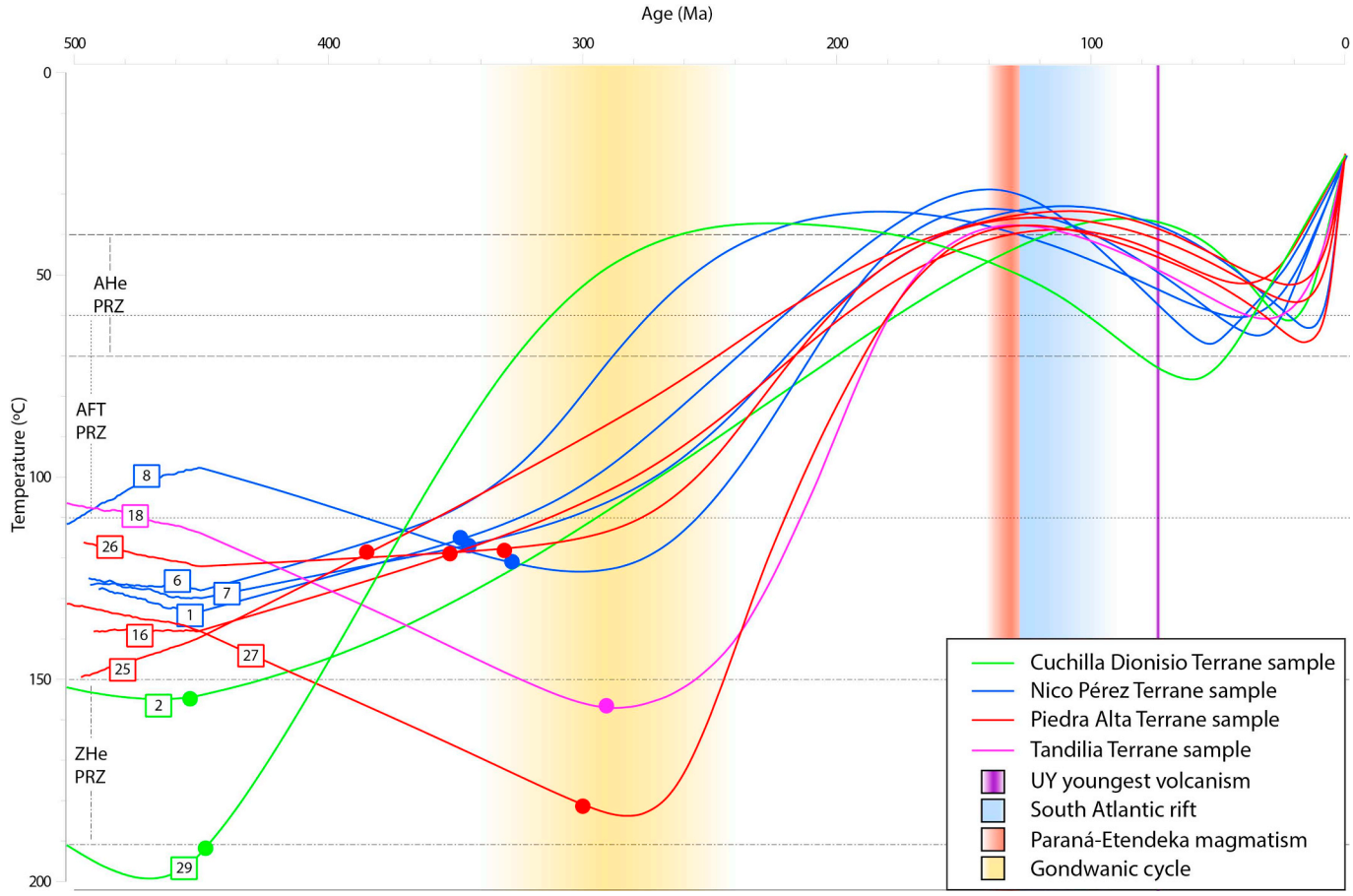

Fig. 8. Mean cooling trajectories of inverse models for samples from Group 1, with sample number indicated. Dots represent point after which trajectory relative probability is over 50% inside the confidence interval. *i.e.* model curve before the dot is poorly constrained. Approximate interval of PRZ of each thermochronometer indicated with dashed horizontal lines. Main thermotectonic events in the region are indicated as shaded bars: Gondwanic cycle (c. 340 to 250 Ma) (Milani and Wit, 2008), Paraná-Etendeka LIP (138 to 125 Ma) (Rossetti et al., 2014) and Atlantic Ocean opening (130 to 113 Ma) (Stica et al., 2014). See Supplementary material for the complete models with the 95% confidence interval.

in young ages owing to rapid He escape. Because a zircon's eU is usually one or two orders of magnitude higher than an apatite's eU, the connection between radioactive defects within the crystal lattice after long-term residence at shallow temperatures is very likely. Therefore, although our ZHe ages tend to be younger than the ones obtained by Hueck et al. (2017) (late Ediacaran to Ordovician), this can be attributed to the difference in the eU of the zircons analyzed in each work. While we found that our dispersed ages have a clear negative correlation with eU, which varies between 299 and 3160 ppm (Fig. 6), Hueck et al. (2017) presented mostly zircons with eU below 500 ppm and whose ZHe ages clustered in the Cambrian. Our low eU samples present very similar ages to those from their work, indicating that most of the UYS reached temperatures within the ZHePRZ in the early Paleozoic. Additionally, the age dispersion observed by us indicates that samples passed through a protracted period of low temperatures (< 150 °C), favoring the accumulation of radiation damage that when interconnected became escape paths for the alpha particles generated within the zircons (Shuster et al., 2006; Reiners et al., 2018).

The evaluation of the thermochronometry ages alone, obtained from the three thermochronometers used in this work and integrated with ages previously published, gives important insights into the thermal behavior of the Uruguayan shield. The higher temperature thermochronometer ZHe ages suggest that most of the shield rocks currently exposed were at temperatures below 200 °C since the early Paleozoic. The AFT data, of intermediate temperature, indicate that samples passed through temperatures between 100 and 60 °C from the late Paleozoic to the middle Mesozoic. Finally, the lower temperature thermochronometer AHe suggests that our samples have been accumulating considerable amounts of radiation damage since the late Paleozoic, and that magmatic events in the region, such as the Paraná-Etendeka LIP and the South Atlantic rift, did not raise basement temperatures to the point of resetting AHe ages (> 70 °C). Nonetheless, AHe ages dispersion and inverse modeling of the thermal history of our samples suggest that these plate-wide events might have increased UYS temperature during Late Cretaceous, as discussed below.

5.2. Thermotectonic evolution of Uruguay

Previous thermotectonic models proposed for the UYS infer a complex thermal history for the now exposed basement rocks, but are not consistent regarding the timing of cooling/reheating phases and exhumation/burial events. In brief, the models of Kollenz (2015), based on AFT data, support cooling towards near-surface conditions (T < 30 °C) from Carboniferous to Jurassic, followed by reheating (up to 65 °C) in the Cretaceous and a final cooling to surface temperature during Cenozoic. The AFT models of Gomes and Almeida (2019) suggest a major cooling phase until the Triassic, reaching temperatures around 60 °C and occasionally showing minor reheating during the late Mesozoic, until a final cooling phase starting in the Miocene. On the other hand, the models of Hueck et al. (2017), based on (U−Th)/He data, suggest cooling to near-surface conditions by the Silurian, followed by shallow reburial (with reheat below 90 °C) and exhumation cycles until Permian and a final cooling to surface temperature during Mesozoic. Despite the conflict on the timing and duration of the cooling

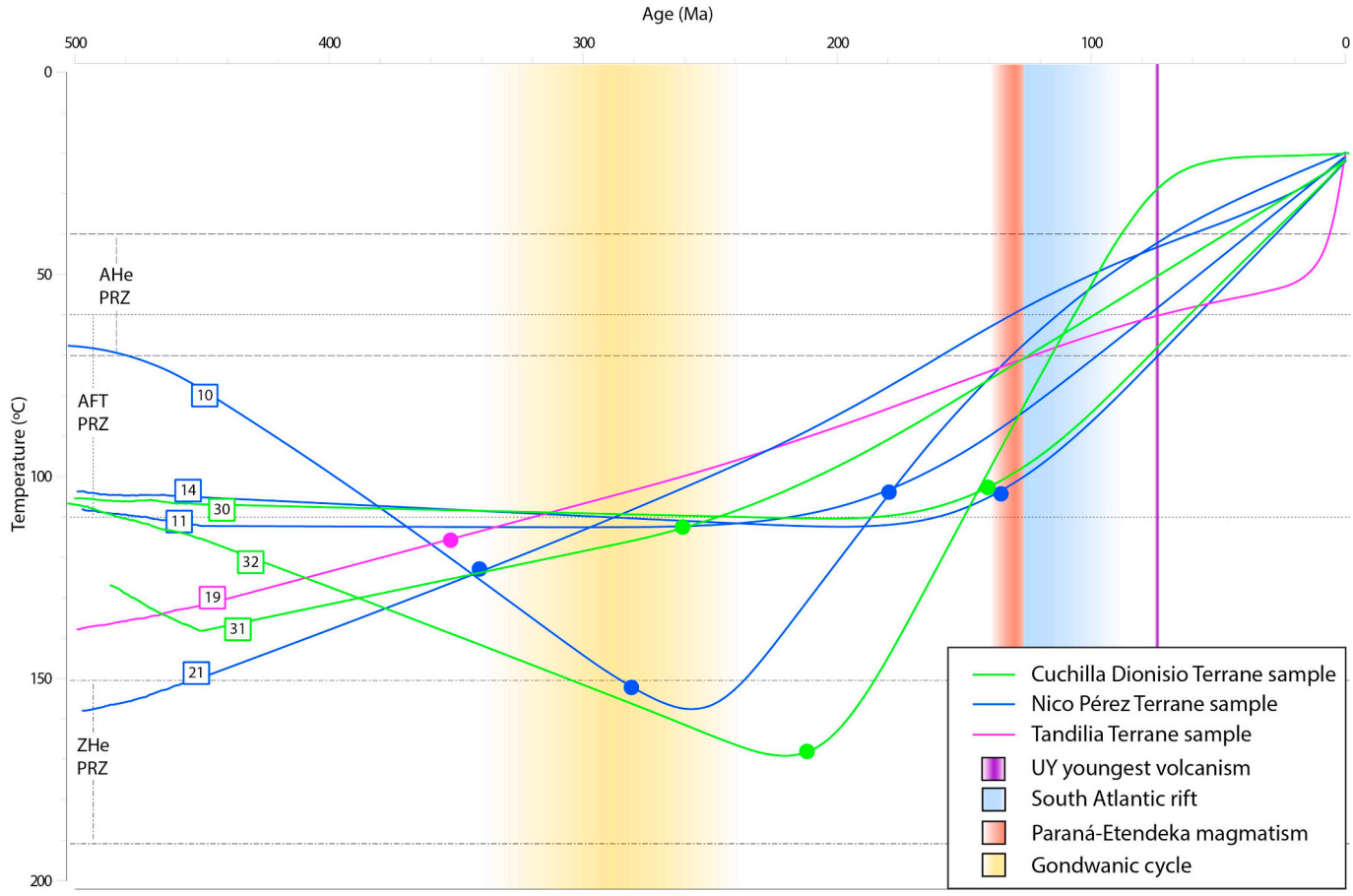

Fig. 9. Mean cooling trajectories of inverse models for samples from Group 2, with sample number indicated. Dots represent point after which trajectory relative probability is over 50% inside the confidence interval. *i.e.* model curve before the dot is poorly constrained. Approximate interval of PRZ of each thermochronometer indicated with dashed horizontal lines. Main thermotectonic events in the region are indicated as shaded bars: Gondwanic cycle (c. 340 to 250 Ma) (Milani and Wit, 2008), Paraná-Etendeka LIP (138 to 125 Ma) (Rossetti et al., 2014) and Atlantic Ocean opening (130 to 113 Ma) (Stica et al., 2014). See Supplementary material for the complete models with the 95% confidence interval.

phases, all authors support a complex thermal history for the region, with a dominant Paleo- Mesozoic cooling phase to temperatures close or below 60 °C, minor reheating episodes or protracted stability near this temperature, and a final Meso-Cenozoic cooling towards surface temperature. Conspicuously, their models were made using different data and user constraints, and their cooling/heating phases imply distinct thermotectonic histories for the UYS. Here, using the information from the previous studies, new AFT, AHe and ZHe data, and models run with more than one thermochronometer and the minimum of user constraints, we suggest a more embracing thermotectonic history for Uruguay.

Based on ZHe and AHe data, Hueck et al. (2017) argued that the shield reached near-surface conditions (< 60 °C) in the Silurian and went through subsidence and exhumation cycles during the Paleozoic, related to deposition of Devonian and Permian Paraná Basin sequences over the UYS. According to the authors, these depositional cycles of shallow burial and erosion did not increase basement temperatures over 90 °C. However, models based on AFT data by Kollenz (2015) and Gomes and Almeida (2019), as well as the multi-thermochronometers models presented here, suggest that most of the shield cooled from the high end of the AFTPAZ (110 °C) only from the Carboniferous onwards. Therefore, if the UYS rocks were exposed to near surface conditions during the Silurian, a reheating to temperatures above the 110 °C would be necessary to reset the AFT thermochronometer during the Devonian.

Deposits of the Durazno Group, part of the Devonian Paraná Supersequence, are exposed in the shield NNE and overlie the eastern PAT and western NPT. Provenance studies by Uriz et al. (2016) support the CDT as the main source for the Durazno Group sediments, which corroborates the early onset of cooling and exhumation observed in our models for CDT samples UY2 and UY29. These models, which include ZHe, suggest temperatures above 150 °C during the Silurian, followed by continuous cooling and exhumation of the samples towards the surface. Thus, the exposure of the CDT to near surface conditions during the Silurian followed by reburial in the Devonian to reset the AFT thermochronometer ($T > 110$ °C) seems unlikely. The Durazno Group would have been deposited on a rather narrow and N-S oriented depression over the PAT and NPT terranes, which also acted as secondary and proximal detrital sources (Uriz et al., 2016). In our models, the onset of cooling for these two terranes occurs around the Devonian-Carboniferous boundary, so they could have been exposed to near surface conditions during the Silurian and buried by the Durazno Group to temperatures over 110 °C to reset their AFT ages during the Devonian. However, our models for these terranes favor a simpler cooling history, fitting Mesozoic AFT ages with ZHe ages as old as Ordovician in the NPT or young as Permian in the PAT, without the need of exposure to the surface during the Silurian and burial in the Devonian. Moreover, palynomorphs and organic matter in the Durazno Group show little thermal overprint, with palynomorph colors ranging from yellow to yellowish brown (Daners et al., 2017), which correspond to diagenetic temperatures below 50 °C (Thermal Alteration Index of 1+ to 2-, Hunt, 1996). All things considered and adopting an Occam's razor principle, exposure of our samples (thus of the UYS) to near surface conditions in the Silurian followed by reset of AFT ages in Devonian seems unlikely, and a continuous protracted cooling of the shield since early to middle

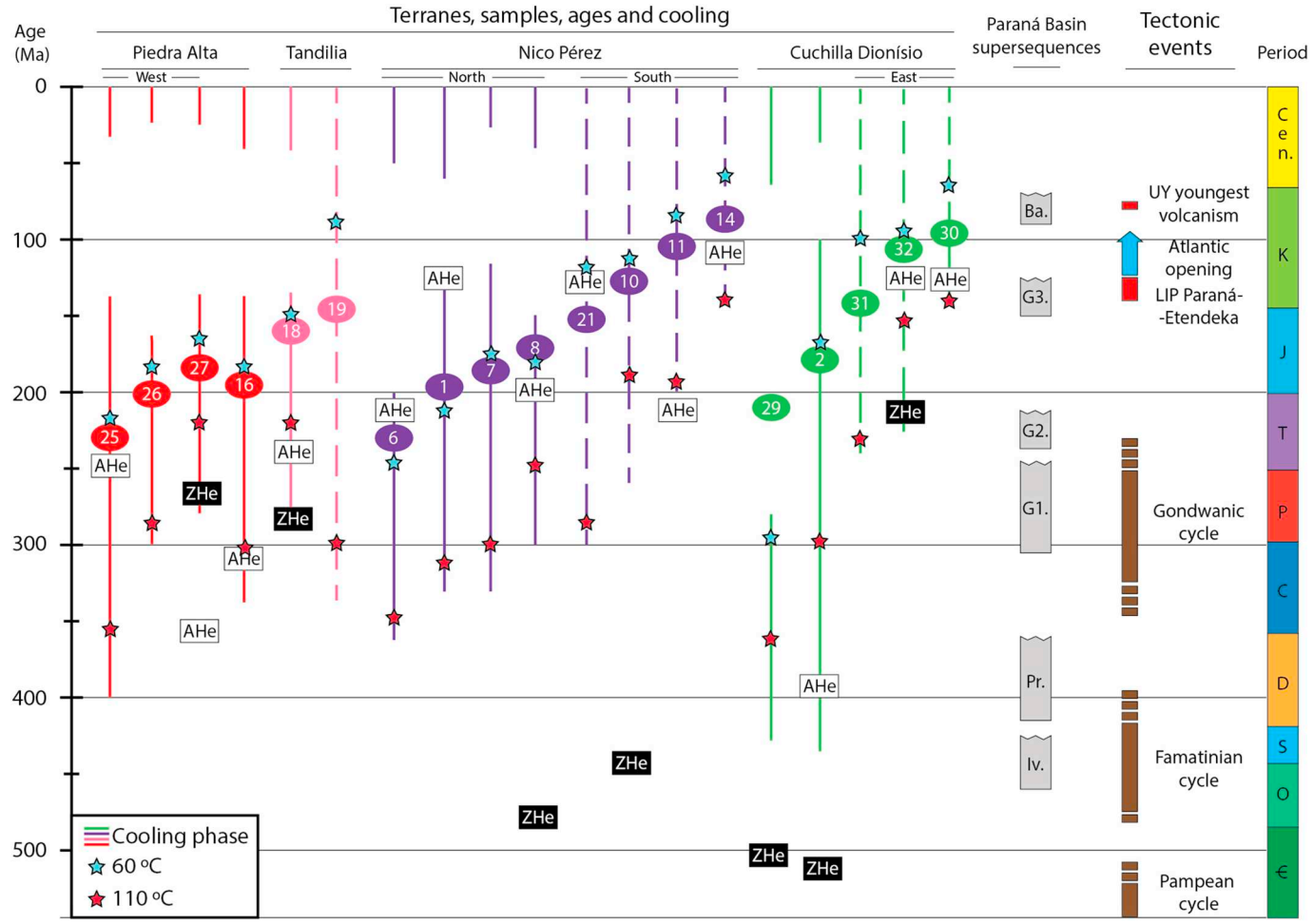

Fig. 10. Chronological chart of cooling phases in the Uruguayan shield observed in inverse thermal models. Solid lines represent cooling of samples from Group 1, dashed lines from Group 2. Sample ID placed according to its AFT central age, while the oldest ZHe and youngest AHe corrected ages are reported when available. Red and blue stars indicate the approximated time of passage through temperatures of 110 and 60 °C, respectively, during the sample's main cooling phase. Boxes on the right represent, tectonic and magmatic regional events in the vicinity of the UYS, and the sedimentary record of the Paraná Basin (supergroups Rio Ivaí - Iv., Paraná - Pr., Gondwana I - G1, Gondwana II - G2, Gondwana III - G3, and Bauru - Ba). (For interpretation of the references to colour in this figure legend, the reader is referred to the web version of this article.)

Paleozoic until the Mesozoic provide a satisfactory fit to the available data, with onset of cooling occurring earlier in the CDT than in the NPT and PAT.

The main cooling phase that led most of the shield rocks to near surface conditions seems to have started during the Carboniferous-Permian transition (Fig. 10). This denudation-induced cooling is characteristic of models from Group 1 (Fig. 8), in which most samples pass through the AFTPAZ (from 110 to 60 °C) between *c.* 300 Ma and the Middle Jurassic. This behavior is consistent over the PAT, TT and north of the NPT, but less constrained on the CDT, where samples went through cooling since early Paleozoic (UY2 and UY29) or later in the Mesozoic (UY30, UY31 and UY32). Continuous cooling from late Paleozoic to middle Mesozoic is also dominant in AFT models from Kollenz (2015) and Gomes and Almeida (2019), although some samples from the latter suggest subtle reheating in this period. The onset of this cooling phase is correlated to the Gondwanic cycle, characterized by subduction of the Panthalassa Ocean and accretion of exotic terranes on the SW margin of Gondwana (Fig. 1) (Scotese et al., 1999; Milani and Wit, 2008). Intraplate stress transmission linked to these collisions reactivated basement structures below the Paraná Basin and surrounding areas (Milani and Wit, 2008), with deformation and exhumation inferred from NE Argentina to southern Brazil until the Triassic (Zambrano and Urien, 1970; Zerfass et al., 2004; Pankhurst et al., 2006; Oliveira et al., 2016; Machado et al., 2019). Therefore, the onset of this major cooling phase in the UYS is likely related to far field propagation stress and deformation caused by the Gondwanic cycle. Moreover, Permian units of the Paraná Basin (Gondwana I Supersequence) are thicker towards the NW Uruguay (De Santa Ana et al., 2006), display paleocurrents preferentially to west and NW, and coarse alluvial deposits in the upper formations, suggesting that the Uruguayan shield was a basement high and possibly a limit for deposition of the Paraná Basin in the late Paleozoic (De Santa Ana, 2004). However, restricted sedimentation and burial of parts of the UYS might have occurred as well, and could explain local reheating observed in some models from Gomes and Almeida (2019).

This main cooling phase of the UYS seems to have persisted until the Late Jurassic, when models suggest that our samples reached near surface temperatures (< 60 °C) (Fig. 8). The Rio de la Plata Craton was probably exposed during the Early Cretaceous, as indicated by the nature of fluvial and aeolian sandstones (Gondwana III Supersequence) present in NW Uruguay (Sprechmann et al., 1981; De Santa Ana, 2004). The continuous and protracted cooling of the UYS, the beginning of which is likely related to intraplate deformation caused by the Gondwanic cycle in the Late Paleozoic, might have continued in the Mesozoic because the uplift of the lithosphere preceding the South Atlantic opening (Early Cretaceous). Such uplift was recorded in the Brazilian margin during the Mesozoic, proposed to be related to lithosphere thinning before Gondwana breakup (Tello Saenz et al., 2003; Zalán,

2004; Carneiro et al., 2012). In southernmost Brazil, cooling contemporaneous to the one found in the UYS was observed in thermochronology studies (Oliveira et al., 2016; Machado et al., 2019) and can be attributed to increased buoyancy of the lithosphere before rifting, possibly caused by the accumulation of melt in the asthenosphere underneath (Quirk and Rüpke, 2018). Remarkably, in the Early Cretaceous the voluminous magmatism of the Paraná-Etendeka Large Igneous Province extruded over most of the Paraná Basin, with lava flows extending from NE Argentina to central Brazil and Paraguay, and correlative units in southern Africa (Zambrano and Urien, 1970; Turner et al., 1994; Gibson et al., 2006). This magmatism is often associated with the presence of the Tristão da Cunha mantle plume under the region and had its peak at *c.* 133 Ma, closely preceding the opening of the South Atlantic Ocean (Turner et al., 1994; Meisling et al., 2001; Gibson et al., 2006; Rossetti et al., 2014). Therefore, the thinning of the lithosphere and the concentration of melt under it in the region between NE Argentina and southern Brazil might have caused the Mesozoic uplift observed in Uruguay.

Rifting in the South Atlantic Ocean propagated from south to north, and is characterized by intense volcanic activity around the UYS. Besides the Paraná-Etendeka LIP magmatism that covered northern Uruguay, the eastern Uruguayan continental margin is domain of the oceanic Pelotas Basin, which possesses broad wedges of magmatic seaward-dipping reflectors, that thicknesses might reach more than a dozen kilometers and width up to one hundred (Soto et al., 2011; Morales et al., 2017; Reuber et al., 2019). Moreover, the spreading rates between South America and Africa increased continuously from 20 mm/yr at *c.* 125 Ma to a peak of 77 mm/yr at *c.* 80 Ma (Granot and Dyment, 2015; Brune et al., 2016), implying in intense magmatic activity at the east of Uruguay. Furthermore, the tectonic stresses related to rifting are thought to have provoked the development of the SaLAM basins, a SW-NE oriented corridor within the shield considered to be an aborted rift precursor to the South Atlantic opening (Rossello et al., 2007). The Laguna Merín Basin, NE sector of the SaLAM, is filled with igneous rocks dated between 134 and 127 Ma (Cernuschi et al., 2015). Therefore, during the Cretaceous, the shield was surrounded by active magmatism and likely lying above the Tristão da Cunha plume influence area. It is plausible that this magmatic context had a thermal effect on the UYS, probably increasing the regional geothermal gradient. Alternatively, Kollenz (2015) suggests that the shield might have had its temperature increased due to partial and shallow burial by lava flows. A reheating episode starting around 140 Ma is suggested by our models from Group 1, with temperatures increasing from surface conditions to about 60 °C during Paleogene. It has been argued that such a reheating phase is a modeling artifact caused by problems related to annealing of fission tracks on temperatures below 60 °C on geological timescales (Jonckheere, 2003), and because it is at the limit of resolution of the AFT system, thus poorly constrained. However, the coincidence in time between the beginning of this reheating phase suggested by the models and the magmatic events surrounding the UYS is notable. Moreover, our set of disperse and old AHe ages argue in favor of a slight reheat to temperatures < 70 °C (Shuster et al., 2006). Therefore, the subtle reheating of the UYS during the Late Cretaceous suggested by the inverse models is supported by evidence of contemporaneous magmatism in the vicinity of the shield. The dispersion of the AHe ages might result from such a reheating phase, as well as the difficulty of the models to fit these ages and constrain the thermal path at temperatures below 60° C. This might arise from the RDAAM kinetic model (Flowers et al., 2009) assumes that the annealing of the alpha-recoil damage is similar to the annealing of fission tracks, what has been questioned recently (*e.g.* Fox and Shuster, 2014; Willett et al., 2017).

The duration and magnitude of the reheating phase cannot be constrained by our data, but the models suggest that regional cooling took place in late Paleogene. This final cooling can simply represent the thermal stabilization of the region to lower temperatures after the intense magmatism during the Cretaceous. The low topography of the UYS suggests an absence of major uplift in the region during the Cenozoic, and our models support that the basement was already near surface conditions before the rifting. However, the accelerated development of the Rio Grande Cone (Morales et al., 2017; Schattner et al., 2019), an offshore feature of the Pelotas Basin located near the boundary between Uruguay and Brazil, begins during the Miocene. Therefore, some uplift of the UYS in the last *c.* 40 Ma cannot be ruled out, as it would provide the sedimentary input needed for the development of the Rio Grande Cone.

Finally, although our models from Group 2 are in general less robust than Group 1 due to the limited number of confined fission tracks, they concur with cooling to temperatures below 60 °C in the Late Cretaceous, possibly reflecting tectonic adjustments during the final stages of the South Atlantic Oceanic opening, including acid volcanism dated at 77 ± 1 Ma in the southern NPT (Gaucher et al., 2016). Samples from Group 2 are located mostly in the eastern margin of the shield or near ancient faults and shear zones of the NPT. The Brasiliano/Pan-African structures within UYS played an important role during the rifting along the South American coast (Oriolo et al., 2018; Schmitt et al., 2018), and the cooling observed in the models from Group 2 might be linked to reactivations of ancient structures. For example, K−Ar ages on fault gouge revealed tectonic activity in the Sierra Ballena Shear Zone during Late Cretaceous, being related to the Gondwana breakup (Hueck et al., 2017).

Therefore, the Gondwana breakup represents a period of intense transformations on the UYS, with movement across old basement structures, intense magmatic events surrounding the shield, and possibly a subtle reheating of the region during the Late Cretaceous. The results and models presented here corroborate previous thermochronometry studies in Uruguay, which used AFT or (U−Th)/He analysis separated, and advance our comprehension about the West Gondwana breakup. Moreover, this work demonstrates that the joint use of different thermochronometers leads to more refined thermal histories. While our data confirm cooling of the UYS below 200 °C in the early Paleozoic, as suggested by the ZHe data from Hueck et al. (2017), it also acknowledges temperatures near or below 60 °C in most of the shield during the middle Mesozoic, supported by AFT data from Kollenz (2015) and Gomes and Almeida (2019). The possible reheating of the UYS, tentatively suggested by the three aforementioned works but poorly constrained by them, is more apparent in our models, and confirm a complex thermal history for Uruguay's basement.

6. Conclusion

In this work we analyzed the thermal behavior of the Uruguayan shield based on information from apatite fission-tracks and apatite and zircon (U−Th)/He thermochronometry. We provided an integrated view of the thermotectonic evolution of the shield, combining 19 new AFT ages, 42 new AHe and 40 new ZHe single crystal ages with data from previous thermochronometry studies. We modeled thermal histories for 19 locations across the UYS and compared the results with previously proposed models. Our main conclusions can be summarized as follows:

1) Most of the shield reached temperatures below 200 °C in the early Paleozoic;
2) Denudation-induced cooling was first observed in samples from the Cuchilla Dionísio Terrane, which provided a major sedimentary source for the Devonian deposits of the Paraná Basin;
3) The main cooling event of the Uruguayan shield began around the Carboniferous-Permian boundary, cooling our samples from temperatures above 100 °C to near surface conditions (< 60 °C) by the Jurassic;
4) The onset of this cooling phase is likely related to far field propagation of tectonic stress associated with the Gondwanic cycle on the SW margin of Gondwana;

5) Lithospheric uplift linked to South Atlantic rifting contributed to the continuity of this cooling phase until the Mesozoic;
6) The magmatic events related to Atlantic Ocean opening likely had a positive thermal effect on the Uruguayan shield, subtly increasing temperatures of the basement rocks during the Late Cretaceous; and.
7) Final cooling to surface temperatures occurred in the Cenozoic, but the rates and timing cannot be precisely constrained by the available thermochronometry data.

CRediT authorship contribution statement

João Pacífico Silveira Luiz Machado:Methodology, Formal analysis, Investigation, Writing - original draft, Visualization, Project administration, Funding acquisition.**Andréa Ritter Jelinek**:Conceptualization, Methodology, Writing - review & editing, Supervision, Funding acquisition.**Randell Stephenson**:Conceptualization, Writing - review & editing, Supervision, Funding acquisition.**Claudio Gaucher**:Investigation, Writing - review & editing.**Marcos Müller Bicca**:Formal analysis, Investigation.**Leticia Chiglino**:Investigation.**Frederico Antonio Genezini**:Formal analysis, Resources.

Declaration of competing interest

The authors declare that they have no known competing financial interests or personal relationships that could have appeared to influence the work reported in this paper.

Acknowledgments

The authors gratefully acknowledge the support from Shell Brasil through the “Shell - BG05: UoA-UFRGS-SWB Sedimentary Systems” project at UFRGS and the strategic importance of the support given by ANP through the R&D levy regulation. We thank Peter Reiners and his team at the Arizona Radiogenic Helium Dating Laboratory (US) for the (U−Th)/He analyses and support during the data evaluation. The first author thanks the CNPq scholarship (SWE 204254/2017-5) during the exchange period at the University of Aberdeen. A.R. Jelinek also thanks the support from CNPq (Project 303184/2017-5). This manuscript was improved after helpful reviews by Mathias Hueck and an anonymous reviewer.

Appendix A. Supplementary data

Supplementary data to this article can be found online at https://doi.org/10.1016/j.tecto.2020.228439.

References

Abre, P., Bossi, J., Cingolani, C., Gaucher, C., Pineyro, D., Blanco, G., 2014. El Terreno Tandilia en Uruguay y Argentina. In: Bossi, J., Gaucher, C. (Eds.), Geología Del Uruguay - Tomo 1: Predevónico, pp. 89–119.

Ault, A.K., Guenthner, W.R., Moser, A.C., Miller, G.H., Refsnider, K.A., 2018. Zircon grain selection reveals (de) coupled metamictization, radiation damage, and He diffusivity. Chem. Geol. 490, 1–12.

Basei, M.A.S., Frimmel, H.E., Nutman, A.P., Preciozzi, F., Jacob, J., 2005. A connection between the Neoproterozoic Dom Feliciano (Brazil/Uruguay) and Gariep (Namibia/South Africa) orogenic belts - evidence from a reconnaissance provenance study. Precambrian Res. 139, 195–221. https://doi.org/10.1016/j.precamres.2005.06.005.

Basei, M.A.S., Peel, E., Sánchez Bettucci, L., Preciozzi, F., Nutman, A.P., 2011. The basement of the Punta del Este Terrane (Uruguay): an African Mesoproterozoic fragment at the eastern border of the South American Río de la Plata Craton. Int. J. Earth Sci. 100, 289–304.

Beri, Á., Gutiérrez, P., Balarino, L., 2011. Palynostratigraphy of the late palaeozoic of Uruguay, paraná basin. Rev. Palaeobot. Palynol. 167, 16–29. https://doi.org/10.1016/j.revpalbo.2011.05.004.

Blanco, G., Rajesh, H.M., Gaucher, C., Germs, G.J.B., Chemale, F., 2009. Provenance of the Arroyo del Soldado Group (Ediacaran to Cambrian, Uruguay): implications for the paleogeographic evolution of southwestern Gondwana. Precambrian Res. 171, 57–73. https://doi.org/10.1016/j.precamres.2009.03.003.

Borba, A.W. de, Vignol-Lelarge, M.L.M., Mizusaki, A.M.P., 2002. Uplift and denudation of the Caçapava do Sul granitoids (southern Brazil) during Late Paleozoic and Mesozoic: constraints from apatite fission-track data. J. S. Am. Earth Sci. 15, 683–692. https://doi.org/10.1016/S0895-9811(02)00086-X.

Borba, A.W. de, Lima, E.F. De, Vignol-Lelarge, M.L.M., Mizusaki, A.M.P., Sparrenberg, I., Barros, C.E.de., 2003. Significance of Late Paleozoic Fission-track Ages in volcanic rocks from the Lavras Do Sul Region, Southernmost Brazil. Gondwana Res. 6, 79–88. https://doi.org/10.1016/S1342-937X(05)70645-6.

Bossi, J., Campal, N., 1992. Magmatismo y tectónica transcurrente durante el Paleozoico Inferior en Uruguay. In: Gutierrez- Marco, J.G., Saavedra, J., Rabano, I. (Eds.), Paleozoico Inferior de Iberoamérica. Mérida, pp. 343–356.

Bossi, J., Cingolani, C., 2009. Extension and general evolution of the Río de la Plata Craton. Developments in Precambrian Geology. https://doi.org/10.1016/S0166-2635(09)01604-1.

Bossi, J., Ferrando, L., 2001. Carta geológica del Uruguay. Escala 1:500.000. Vérsion 2.0–2001. Catedra de Geologia, Facultad de Agronomía.

Bossi, J., Gaucher, C., 2004. The cuchilla dionisio terrane, Uruguay: an allochthonous block accreted in the Cambrian to SW-Gondwana. Gondwana Res. 7, 661–674. https://doi.org/10.1016/S1342-937X(05)71054-6.

Bossi, J., Gaucher, C., 2014a. Estratigrafia del Predevonico del Uruguay. In: Bossi, J., Gaucher, C. (Eds.), *Geología Del Uruguay - Tomo 1: Predevónico*. Montevideo, pp. 19–42.

Bossi, J., Gaucher, C., 2014b. Formacion valentines. In: Bossi, J., Gaucher, C. (Eds.), Geología Del Uruguay - Tomo 1: Predevónico, pp. 171–189.

Bossi, J., Piñeyro, D., 2014. Terreno Piedra Alta. In: Bossi, J., Gaucher, C. (Eds.), *Geología Del Uruguay - Tomo 1: Predevónico*. Montevideo, pp. 43–86.

Bossi, J., Gaucher, C., Chiglino, L., Navarro, R., Piñeyro, D., 2014. Escama Tectonica Carape. In: Bossi, J., Gaucher, C. (Eds.), Geología Del Uruguay - Tomo 1: Predevónico, pp. 265–282.

Brown, R.W., Beucher, R., Roper, S., Persano, C., Stuart, F., Fitzgerald, P., 2013. Natural age dispersion arising from the analysis of broken crystals. Part I: theoretical basis and implications for the apatite (U–Th)/He thermochronometer. Geochim. Cosmochim. Acta 122, 478–497. https://doi.org/10.1016/j.gca.2013.05.041.

Brune, S., Williams, S.E., Butterworth, N.P., Müller, R.D., 2016. Abrupt plate accelerations shape rifted continental margins. Nature 536, 201–204. https://doi.org/10.1038/nature18319.

Carlson, W.D., Donelick, R.A., Ketcham, R.A., 1999. Variability of apatite fission-track annealing kinetics: I. Experimental results. Am. Mineral. 84, 1213–1223. https://doi.org/10.2138/am-1999-0901.

Carneiro, C.D.R., Almeida, F.F.M. de, Hasui, Y., Zalán, P.V., Teixeira, J.B.G., 2012. Estagios Evolutivos do Brasil no Fanerozoico. In: Hasui, Y., Carneiro, C.D.R., Almeida, F.F.M. de, Bartorelli, A. (Eds.), Geologia Do Brasil. Editora Beca, São Paulo, pp. 131–137.

Cernuschi, F., Dilles, J.H., Kent, A.J.R., Schroer, G., Raab, A.K., Conti, B., Muzio, R., 2015. Geology, geochemistry and geochronology of the Cretaceous Lascano East intrusive complex and magmatic evolution of the Laguna Merín basin, Uruguay. Gondwana Res. 28, 837–857. https://doi.org/10.1016/j.gr.2014.07.007.

Chiglino, L., Gaucher, C., Sial, A.N., Bossi, J., Ferreira, V.P., Pimentel, M.M., 2010. Chemostratigraphy of Mesoproterozoic and Neoproterozoic carbonates of the Nico Pérez Terrane, Río de la Plata Craton, Uruguay. Precambrian Res. 182, 313–336.

Cogné, N., Gallagher, K., Cobbold, P.R., 2011. Post-rift reactivation of the onshore margin of southeast Brazil: evidence from apatite (U-Th)/He and fission-track data. Earth Planet. Sci. Lett. 309, 118–130. https://doi.org/10.1016/j.epsl.2011.06.025.

Cogné, N., Gallagher, K., Cobbold, P.R., Riccomini, C., Gautheron, C., 2012. Post-breakup tectonics in southeast Brazil from thermochronological data and combined inverse-forward thermal history modeling. Journal of Geophysical Research B: Solid Earth 117, 1–16. https://doi.org/10.1029/2012JB009340.

Daners, G., Le Herisse, A., Breuer, P., Veroslavsky, G., 2017. Pragian-Emsian palynomorphs from the Cordobés Formation, Norte Basin, Uruguay: stratigraphically restricted and regionally correlative palynological events in the cool-water Malvinokaffric Realm. Palynology 41, 121–137.

de Almeida, F.F.M., Hasui, Y., de Brito Neves, B.B., Fuck, R.A., 1981. Brazilian structural provinces: an introduction. Earth Sci. Rev. 17 (1–2), 1–29.

De Santa Ana, H., 2004. Análise Tectono-Estratigráfica Das Seqüências Chacoparanense Uruguaia (“Cuenca Norte ”). Universidade Estadual Paulista.

De Santa Ana, H., Veroslavsky, G., Fúlfaro, V., Rossello, E., 2006. Cuenca Norte: evolución tectónica y sedimentaria del Carbonífero-Pérmico. In: Veroslavsky, G., Ubilla, M., Martínez, S. (Eds.), Cuencas sedimentarias de Uruguay. Paleozoico. Facultad de Ciencias, Montevideo, pp. 209–244.

Dodson, M.H., 1973. Closure temperature in cooling geochronological and petrological systems. Contrib. Mineral. Petrol. 40, 259–274. https://doi.org/10.1007/BF00373790.

Donelick, R.A., 1993. Method of Fission Track Analysis Utilizing Bulk Chemical Etching of Apatite. 35.

Donelick, R.A., Ketcham, R.A., Carlson, W.D., 1999. Variability of apatite fission-track annealing kinetics: II. Crystallographic orientation effects. Am. Mineral. 84, 1224–1234. https://doi.org/10.2138/am-1999-0902.

Donelick, R.A., O’Sullivan, P.B., Ketcham, R.A., 2005. Apatite Fission-Track analysis. In: Reiners, P.W., Ehlers, T.A. (Eds.), Low-temperature Thermochronology: Techniques, Interpretations, and Applications. Mineralogical Society of America, pp. 49–94.

Faraone, M., 2018. Geología, petrografía y aspectos estructurales del extremo sur-occidental de la Zona de Cizalla Sarandí del Yí (área SW de Solís de Mataojo). Degree Thesis. Facultad de Ciencias, Montevideo.

Farley, K.A., 2000. Helium diffusion from apatite: general behavior as illustrated by Durango fluorapatite. Journal of Geophysical Research: Solid Earth 105, 2903–2914. https://doi.org/10.1029/1999JB900348.

Farley, K.A., 2002. (U-Th)/He dating: techniques, calibrations, and applications. Rev. Mineral. Geochem. 47, 819–844. https://doi.org/10.2138/rmg.2002.47.18.
Farley, K.A., Wolf, R.A., Silver, L.T., 1996. The effects of long alpha-stopping distances on (U-Th)/He ages. Geochim. Cosmochim. Acta 60, 4223–4229. https://doi.org/10.1016/S0016-7037(96)00193-7.
Fernandes, L.A.D.A., Koester, E., 1999. The Neoproterozoic Dorsal de Cangucu strike-slip shear zone: its nature and role in the tectonic evolution of southern Brazil. J. Afr. Earth Sci. 29, 3–24. https://doi.org/10.1016/S0899-5362(99)00076-7.
Fernandes, L.A.D.A., Tommasi, A., Vauchez, A., Porcher, C.C., Menegat, R., Koester, E., 1993. Zona De Cisalhamento Transcorrente Dorsal De Canguçu: Caracterização E Importância Na Compartimentação Tectônica Do Cinturão Dom Feliciano. Revista Brasileira de Geociências 23, 224–233. https://doi.org/10.25249/0375-7536.1993233224233.
Fernandes, L.A.D.A., MENEGAT, R., et al., 1995. Evolução Tectônica Do Cinturão Dom Feliciano No Escudo Sul-Rio-Grandense: Parte L - Uma Contribuição A Partir Do Registro Geológico. Revista Brasileira de Geociências 25, 351–374. https://doi.org/10.25249/0375-7536.1995351374.
Fleischer, R.L., Price, P.B., Walker, R.M., 1975. Nuclear Tracks in Solids: Principles and Applications. University of California Press, California.
Flowers, R.M., Kelley, S.A., 2011. Interpreting data dispersion and ‘ inverted’ dates in apatite (U-Th)/He and fission-track datasets: an example from the US midcontinent. Geochim. Cosmochim. Acta 75, 5169–5186. https://doi.org/10.1016/j.gca.2011.06.016.
Flowers, R.M., Shuster, D.L., Wernicke, B.P., Farley, K.A., 2007. Radiation damage control on apatite (U-Th)/He dates from the Grand Canyon region, Colorado Plateau. Geology 35, 447. https://doi.org/10.1130/G23471A.1.
Flowers, R.M., Ketcham, R.A., Shuster, D.L., Farley, K.A., 2009. Apatite (U-Th)/He thermochronometry using a radiation damage accumulation and annealing model. Geochim. Cosmochim. Acta 73, 2347–2365. https://doi.org/10.1016/j.gca.2009.01.015.
Fox, M., Shuster, D.L., 2014. The influence of burial heating on the (U–Th)/He system in apatite: Grand Canyon case study. Earth Planet. Sci. Lett. 397, 174–183.
Galbraith, R.F., 1981. On statistical models for fission track counts. J. Int. Assoc. Math. Geol. 13, 471–478. https://doi.org/10.1007/BF01034498.
Galbraith, R.F., Green, P.F., 1990. Estimating the component ages in a finite mixture. International Journal of Radiation Applications and Instrumentation. Part D. Nuclear Tracks and Radiation Measurements 17, 197–206. https://doi.org/10.1016/1359-0189(90)90035-V.
Galbraith, R.F., Laslett, G.M., Green, P.F., Duddy, I.R., 1990. Apatite fission track analysis: geological thermal history analysis based on a three-dimensional random process of linear radiation damage. Philosophical Transactions of the Royal Society of London. Series A: Physical and Engineering Sciences 332, 419–438. https://doi.org/10.1098/rsta.1990.0124.
Gallagher, K., 2012. Transdimensional inverse thermal history modeling for quantitative thermochronology. Journal of Geophysical Research: Solid Earth 117, 1–16. https://doi.org/10.1029/2011JB008825.
Gallagher, K., Brown, R., 1997. The onshore record of passive margin evolution. J. Geol. Soc. 154, 451–457. https://doi.org/10.1144/gsjgs.154.3.0451.
Gallagher, K., Brown, R.W., 1999. The Mesozoic denudation history of the Atlantic margins of southern Africa and southeast Brazil and the relationship to offshore sedimentation. Geol. Soc. Lond., Spec. Publ. 153, 41–53. https://doi.org/10.1144/GSL.SP.1999.153.01.03.
Gallagher, K., Hawkesworth, C.J., Mantovani, M.S.M., 1994. The denudation history of the onshore continental margin of SE Brazil inferred from apatite fission track data. Journal of Geophysical Research: Solid Earth 99, 18117–18145. https://doi.org/10.1029/94JB00661.
Gallagher, K., Hawkesworth, C.J., Mantovani, M.S.M., 1995. Denudation, fission track analysis and the long-term evolution of passive margin topography: application to the southeast Brazilian margin. J. S. Am. Earth Sci. 8, 65–77. https://doi.org/10.1016/0895-9811(94)00042-Z.
Gallagher, K., Charvin, K., Nielsen, S., Sambridge, M., Stephenson, J., 2009. Markov chain Monte Carlo (MCMC) sampling methods to determine optimal models , model resolution and model choice for Earth Science problems. Mar. Pet. Geol. 26, 525–535. https://doi.org/10.1016/j.marpetgeo.2009.01.003.
Gaucher, C., 2000. Sedimentology, palaeontology and stratigraphy of the Arroyo del Soldado Group (Vendian to Cambrian, Uruguay). Beringeria 26, 1–120.
Gaucher, C., Nóbrega Sial, A., Blanco, G., Sprechmann, P., 2004. Chemostratigraphy of the lower Arroyo del soldado group (Vendian, Uruguay) and palaeoclimatic implications. Gondwana Res. 7, 715–730. https://doi.org/10.1016/S1342-937X(05)71058-3.
Gaucher, C., Finney, S.C., Poiré, D.G., Valencia, V.A., Grove, M., Blanco, G., Pamoukaghlián, K., Gómez Peral, L., 2008. Detrital zircon ages of Neoproterozoic sedimentary successions in Uruguay and Argentina: insights into the geological evolution of the Río de la Plata Craton. Precambrian Res. 167, 150–170.
Gaucher, C., Bossi, J., Blanco, G., 2009a. Palaeogeography. Neoproterozoic-Cambrian evolution of the Río de la Plata Palaeocontinent. In: Gaucher, C., Sial, A.N., Halverson, G.P., Frimmel, H.E. (Eds.), Neoproterozoic-Cambrian Tectonics, Global Change and Evolution: A Focus on Southwestern Gondwana. Developments in Precambrian Geology. 16. Elsevier, pp. 131–141.
Gaucher, C., Frimmel, H.E., Germs, G.J.B., 2009b. Tectonic events and palaeogeographic evolution of southwestern Gondwana in the Neoproterozoic and Cambrian. In: Gaucher, C., Sial, A.N., Halverson, G.P., Frimmel, H.E. (Eds.), Neoproterozoic-Cambrian Tectonics, Global Change and Evolution: A Focus on Southwestern Gondwana. Developments in Precambrian Geology. 16. Elsevier, pp. 295–316.
Gaucher, C., Chemale, F., Bossi, J., Castiglioni, E.A., 2010. Grupo Cebollattí, Tererno Nico Perez: definición y edad. VI Congreso Uruguayo de Geología, Minas.
Gaucher, C., Frei, R., et al., 2011. Mesoproterozoic evolution of the Río de la Plata Craton in Uruguay: at the heart of Rodinia? Int. J. Earth Sci. 100, 273–288. https://doi.org/10.1007/s00531-010-0562-x.
Gaucher, C., Frei, R., Sial, A.N., Castiglioni, E., Ferreira, V.P., 2014. Grupo Cebollatí. In: Bossi, J., Gaucher, C. (Eds.), Geología del Uruguay. Tomo 1: Predevónico, pp. 155–169 Polo, Montevideo.
Gaucher, C., Babinski, M., Blanco, G., 2016. Riolitas del Cretácico Superior (Campaniense); el magmatismo más joven de Uruguay. VIII Congreso Uruguayo de Geología, Actas, Montevideo, pp. 160–161.
Gibson, S.A., Thompson, R.N., Day, J.A., 2006. Timescales and mechanisms of plume-lithosphere interactions: 40Ar/39Ar geochronology and geochemistry of alkaline igneous rocks from the Paraná-Etendeka large igneous province. Earth Planet. Sci. Lett. 251, 1–17. https://doi.org/10.1016/j.epsl.2006.08.004.
Gleadow, A.J.W., 1981. Fission-track dating methods: what are the real alternatives? Nuclear Tracks 5, 3–14. https://doi.org/10.1016/0191-278X(81)90021-4.
Gleadow, A.J.W., Duddy, I.R., Green, P.F., Lovering, J.F., 1986a. Confined fission track lengths in apatite: a diagnostic tool for thermal history analysis. Contrib. Mineral. Petrol. 94, 405–415. https://doi.org/10.1007/BF00376334.
Gleadow, A.J.W., Duddy, I.R., Green, P.F., Hegarty, K.A., 1986b. Fission track lengths in the apatite annealing zone and the interpretation of mixed ages. Earth Planet. Sci. Lett. 78, 245–254. https://doi.org/10.1016/0012-821X(86)90065-8.
Gomes, C.H., Almeida, D., 2019. New insights into the Gondwana breakup at the Southern South America by apatite fission-track analyses. Adv. Geosci. 47, 1–15. https://doi.org/10.5194/adgeo-47-1-2019.
Granot, R., Dyment, J., 2015. The Cretaceous opening of the South Atlantic Ocean. Earth Planet. Sci. Lett. 414, 156–163. https://doi.org/10.1016/j.epsl.2015.01.015.
Green, P.F., 1986. On the thermo-tectonic evolution of Northern England: evidence from fission track analysis. Geol. Mag. 123, 493–506. https://doi.org/10.1017/S0016756800035081.
Green, P.F., Duddy, I., 2018. Apatite (U–Th–Sm)/He Thermochronology on the Wrong Side of the Tracks. 488. pp. 21–33. https://doi.org/10.1016/j.chemgeo.2018.04.028.
Green, P.F., Duddy, I.R., 2006. Interpretation of apatite (U–Th)/He ages and fission track ages from cratons. Earth Planet. Sci. Lett. 244, 541–547. https://doi.org/10.1016/j.epsl.2006.02.024.
Green, P.F., Crowhurst, P.V., Duddy, I.R., Japsen, P., Holford, S.P., 2006. Conflicting (U–Th)/He and fission track ages in apatite: enhanced He retention, not anomalous annealing behaviour. Earth Planet. Sci. Lett. 250 (3–4), 407–427.
Guenthner, W.R., Reiners, P.W., Ketcham, R.A., Nasdala, L., Giester, G., 2013. Helium diffusion in natural zircon: radiation damage, anisotropy, and the interpretation of zircon (U-TH)/He thermochronology. Am. J. Sci. 313, 145–198. https://doi.org/10.2475/03.2013.01.
Hackspacher, P.C., Ribeiro, L.F.B., Ribeiro, M.C.S., Fetter, A.H., Hadler Neto, J.C., Tello, C.E.S., Dantas, E.L., 2004. Consolidation and break-up of the South American Platform in southeastern Brazil: tectonothermal and denudation histories. Gondwana Res. 7, 91–101. https://doi.org/10.1016/S1342-937X(05)70308-7.
Hartmann, L.A., Campal, N., Santos, J.O.S., McNaughton, N.J., Bossi, J., Schipilov, A., Lafon, J.M., 2001. Archean crust in the Rio de la Plata Craton, Uruguay - SHRIMP U-Pb zircon reconnaissance geochronology. J. S. Am. Earth Sci. 14, 557–570. https://doi.org/10.1016/S0895-9811(01)00055-4.
Hartmann, L.A., Santos, J.O.S., Cingolani, C.A., McNaughton, N.J., 2002. Two paleoproterozoic orogenies in the evolution of the Tandilia Belt, Buenos Aires, as evidenced by zircon U-Pb SHRIMP geochronology. Int. Geol. Rev. 44, 528–543.
Hasui, Y., 2010. A grande colisão Pré-Cambrian do sudeste brasileiro e a estruturacao regional. Geociências – UNESP 29, 141–169.
Hueck, M., Oriolo, S., et al., 2017. Phanerozoic low-temperature evolution of the Uruguayan Shield along the South American passive margin. J. Geol. Soc. Lond. https://doi.org/10.1144/jgs2016-101.
Hueck, M., Dunkl, I., Heller, B., Angelo, M., Basei, S., Siegesmund, S., 2018a. (U-Th)/He Thermochronology and Zircon Radiation Damage in the South American Passive Margin : Thermal Overprint of the Paraná LIP ? pp. 1–18. https://doi.org/10.1029/2018TC005041.
Hueck, M., Oyhantçabal, P., Philipp, R.P., Angelo, M., Basei, S., Siegesmund, S., 2018b. In: Siegesmund, S., Basei, M.A.S., Oyhantçabal, P., Oriolo, S. (Eds.), The Dom Feliciano Belt in Southern Brazil and Uruguay. Springer International Publishing, Regional Geology Reviews, Cham. https://doi.org/10.1007/978-3-319-68920-3.
Hunt, J.M., 1996. Petroleum Geochemistry and Geology, Second edition. W.H. Freeman & Co, New York, pp. 1–743.
Hurford, A.J., 1990. Standardization of fission-track dating calibration - recommendation by the Fission-Track Working Group of the Iugs Subcommission on Geochronology. Chem. Geol. 80, 171–178 (ST-Standardization of Fission-Track Dat).
Hurford, A.J., Green, P.F., 1983. The zeta age calibration of fission-track dating. Chem. Geol. 41, 285–317. https://doi.org/10.1016/S0009-2541(83)80026-6.
Jelinek, A.R., Cezar, A., Neto, B., Poupeau, G., 2003. Análise Por Traços De Fissão Em Apatitas Do Distrito Fluorítico De Santa Catarina: Relações Entre Hidrotermalismo E Evolução Da Margem Continental. Recherche 33, 289–298.
Jonckheere, R., 2003. On methodical problems in estimating geological temperature and time from measurements of fission tracks in apatite. Radiat. Meas. 36, 43–55. https://doi.org/10.1016/S1350-4487(03)00096-9.
Karl, M., Glasmacher, U.A., Kollenz, S., Franco-Magalhaes, A.O.B., Stockli, D.F., Hackspacher, P.C., 2013. Evolution of the South Atlantic passive continental margin in southern Brazil derived from zircon and apatite (U-Th-Sm)/He and fission-track data. Tectonophysics 604, 224–244. https://doi.org/10.1016/j.tecto.2013.06.017.
Ketcham, R.A., Carter, A., Donelick, R.A., Barbarand, J., Hurford, A.J., 2007. Improved modeling of fission-track annealing in apatite. Am. Mineral. 92, 799–810. https://doi.org/10.2138/am.2007.2281.

Kollenz, S., 2015. Long-term Landscape Evolution, Cooling and Exhumation History of the South American Passive Continental Margin in NE Argentina & SW Uruguay.
Kollenz, S., Glasmacher, U.A., Rossello, E.A., Stockli, D.F., Schad, S., Pereyra, R.E., 2017. Thermochronological constraints on the Cambrian to recent geological evolution of the Argentina passive continental margin. Tectonophysics 716, 182–203. https://doi.org/10.1016/j.tecto.2016.11.019.
Krob, F.C., Glasmacher, U.A., Karl, M., Perner, M., Hackspacher, P.C., Stockli, D.F., 2019. Multi-chronometer thermochronological modelling of the Late Neoproterozoic to recent t-T-evolution of the SE coastal region of Brazil. J. S. Am. Earth Sci. 92, 77–94. https://doi.org/10.1016/j.jsames.2019.02.012.
Machado, J.P.S.L., Jelinek, A.R., Bicca, M.M., Stephenson, R., Genezini, F.A., 2019. West Gondwana orogenies and Pangaea breakup: thermotectonic effects on the southern-most Mantiqueira Province, Brazil. J. Geol. Soc., jgs2019-018. https://doi.org/10.1144/jgs2019-018.
Mallmann, G., Chemale, F., Ávila, J.N., Kawashita, K., Armstrong, R.A., 2007. Isotope geochemistry and geochronology of the Nico Pérez Terrane, Rio de la Plata Craton, Uruguay. Gondwana Res. 12, 489–508. https://doi.org/10.1016/j.gr.2007.01.002.
Masquelin, H., 2006. El Escudo Uruguayo. In: Cuencas Sedimentarias Del Uruguay. DIRAC Facultad de Ciencias, pp. 37–106.
Meisling, K.E., Cobbold, P.R., Mount, V.S., 2001. Segmentation of an obliquely rifted margin, Campos and Santos basins, southeastern Brazil. AAPG Bull. 85, 1903–1924. https://doi.org/10.1306/8626D0B3-173B-11D7-8645000102C1865D.
Milani, E.J., 1997. Evolução Tectono-Estratigráfica Da Bacia Do Paraná e Seu Relacionamento Com a Geodinâmica Fanerozóica Do Gondwana Sul-Ocidental. Universidade Federal do Rio Grande do Sul.
Milani, E.J., Wit, M.J. De, 2008. Correlations Between the Classic Paraná and Cape − Karoo Sequences of South America and Southern Africa and Their Basin Infills Flanking the Gondwanides : du Toit Revisited and Cape – Karoo Correlations between the Classic Parana Sequences of South Amer. https://doi.org/10.1144/SP294.17.
Milani, E.J., Melo, J.H.G. de, Souza, P.A. De, Fernandes, L.A., França, A.B., 2007. Bacia do Paraná. Boletim de Geociências da Petrobras 8, 265–287.
Morales, E., Chang, H.K., et al., 2017. Tectonic and stratigraphic evolution of the Punta del Este and Pelotas basins (offshore Uruguay). Pet. Geosci. 23, 415–426. https://doi.org/10.1144/petgeo2016-059.
Murray, K.E., Orme, D.A., Reiners, P.W., 2014. Effects of U–Th-rich grain boundary phases on apatite helium ages. Chem. Geol. 390, 135–151. https://doi.org/10.1016/j.chemgeo.2014.09.023.
Nasdala, L., Reiners, P.W., Garver, J.I., Kennedy, A.K., Stern, R.A., Balan, E., Wirth, R., 2004. Incomplete retention of radiation damage in zircon from Sri Lanka. Am. Mineral. 89, 219–231. https://doi.org/10.2138/am-2004-0126.
Nürnberg, D., Müller, R.D., 1991. The tectonic evolution of the South Atlantic from Late Jurassic to present. Tectonophysics 191 (1–2), 27–53.
Oliveira, C.H.E. de, Jelinek, A.R., Chemale, F., Bernet, M., 2016. Evidence of post-Gondwana breakup in Southern Brazilian Shield: insights from apatite and zircon fission track thermochronology. Tectonophysics 666, 173–187. https://doi.org/10.1016/j.tecto.2015.11.005.
Oriolo, S., Oyhantçabal, P., Basei, M.A.S., Wemmer, K., Siegesmund, S., 2016a. The Nico Pérez Terrane (Uruguay): from Archean crustal growth and connections with the Congo Craton to late Neoproterozoic accretion to the Río de la Plata Craton. Precambrian Res. 280, 147–160. https://doi.org/10.1016/j.precamres.2016.04.014.
Oriolo, S., Oyhantçabal, P., et al., 2016b. Timing of deformation in the Sarandí del Yí Shear Zone, Uruguay: Implications for the amalgamation of western Gondwana during the Neoproterozoic Brasiliano-Pan-African Orogeny. Tectonics 35, 754–771. https://doi.org/10.1002/2015TC004052.
Oriolo, S., Hueck, M., Oyhantçabal, P., Goscombe, B., Wemmer, K., Siegesmund, S., 2018. Shear zones in Brasiliano-Pan-African belts and their role in the Amalgamation and break-up of Southwest Gondwana. In: Geology of Southwest Gondwana. Springer International Publishing, pp. 593–613. https://doi.org/10.1007/978-3-319-68920-3.
Oyhantçabal, P., Siegesmund, S., Wemmer, K., 2011. The Río de la Plata Craton: a review of units, boundaries, ages and isotopic signature. Int. J. Earth Sci. 100, 201–220. https://doi.org/10.1007/s00531-010-0580-8.
Oyhantçabal, P., Cingolani, C.A., Wemmer, K., 2018. The Río de La Plata Craton of Argentina and Uruguay. Springer International Publishinghttps://doi.org/10.1007/978-3-319-68920-3.
Oyhantçabal, P.B., Wagner-Eimer, M., Wemmer, K., Schulz, B., Frei, R., Siegesmund, S., 2012. Paleo- and Neoproterozoic magmatic and tectonometamorphic evolution of the Isla Cristalina de Rivera (Nico Pérez Terrane, Uruguay). Int. J. Earth Sci. 101, 1745–1762.
Pamoukaghlián, K., Gaucher, C., Frei, R., Poiré, D.G., Chemale, F., Frei, D., Will, T.M., 2017. U-Pb age constraints for the La Tuna Granite and Montevideo Formation (Paleoproterozoic, Uruguay): unravelling the structure of the Río de la Plata Craton. J. S. Am. Earth Sci. 79, 443–458.
Pankhurst, R.J., Rapela, C.W., Fanning, C.M., Márquez, M., 2006. Gondwanide continental collision and the origin of Patagonia. Earth Sci. Rev. 76, 235–257. https://doi.org/10.1016/j.earscirev.2006.02.001.
Peel, E., Sánchez Bettucci, L., Basei, M.A.S., 2018. Geology and geochronology of Paso del Dragón Complex (northeastern Uruguay): implications on the evolution of the Dom Feliciano Belt (Western Gondwana). J. S. Am. Earth Sci. 85, 250–262.
Pérez-Díaz, L., Eagles, G., 2014. Constraining South Atlantic growth with seafloor spreading data. Tectonics 33 (9), 1848–1873.
Philipp, R.P., Pimentel, M.M., Chemale, F., 2016. Tectonic evolution of the Dom Feliciano Belt in Southern Brazil: geological relationships and U-Pb geochronology. Brazilian Journal of Geology 46, 83–104. https://doi.org/10.1590/2317-4889201620150016.
Philipp, R.P., Pimentel, M.M., Basei, M.A.S., 2018. The tectonic evolution of the São Gabriel Terrane, Dom Feliciano Belt, Southern Brazil: the closure of the Charrua Ocean. In: Geology of Southwest Gondwana. Springer International Publishing, pp. 243–265. https://doi.org/10.1007/978-3-319-68920-3.
Price, P.B., Walker, R.M., 1963. Fossil tracks of charged particles in mica and the age of minerals. J. Geophys. Res. 68, 4847–4862. https://doi.org/10.1029/JZ068i016p04847.
Quirk, D.G., Rüpke, L.H., 2018. Melt-induced buoyancy may explain the elevated rift-rapid sag paradox during breakup of continental plates. Sci. Rep. 8, 1–13. https://doi.org/10.1038/s41598-018-27981-2.
Rapela, C.W., Fanning, C.M., Casquet, C., Pankhurst, R.J., Spalletti, L., Poiré, D., Baldo, E.G., 2011. The Rio de la Plata craton and the adjoining Pan-African/brasiliano terranes: their origins and incorporation into south-west Gondwana. Gondwana Res. 20, 673–690. https://doi.org/10.1016/j.gr.2011.05.001.
Reiners, P.W., 2005. Zircon (U-Th)/He thermochronometry. Rev. Mineral. Geochem. 151–179. https://doi.org/10.2138/rmg.2005.58.6.
Reiners, P.W., Farley, K.A., 2001. Influence of crystal size on apatite (U-Th)/He thermochronology: an example from the Bighorn Mountains, Wyoming. Earth Planet. Sci. Lett. 188, 413–420. https://doi.org/10.1016/S0012-821X(01)00341-7.
Reiners, P.W., Farley, K.A., Hickes, H.J., 2002. He diffusion and (U-Th)/He thermochronometry of zircon: initial results from fish Canyon Tuff and Gold Butte. Tectonophysics 349, 297–308. https://doi.org/10.1016/S0040-1951(02)00058-6.
Reiners, P.W., Spell, T.L., Nicolescu, S., Zanetti, K.A., 2004. Zircon (U-Th)/He thermochronometry: He diffusion and comparisons with 40Ar/39Ar dating. Geochim. Cosmochim. Acta 68, 1857–1887. https://doi.org/10.1016/j.gca.2003.10.021.
Reiners, P.W., Carlson, R.W., Renne, P.R., Cooper, K.M., Granger, D.E., McLean, N.M., Schoene, B., 2018. The (U-Th)He system. In: Geochronology and Thermochronology. John Wiley & Sons Ltd, pp. 291–363.
Reuber, K., Mann, P., Pindell, J., 2019. Hotspot origin for asymmetrical conjugate volcanic margins of the Austral South Atlantic Ocean as imaged on deeply-penetrating seismic reflection images. Interpretation 1–88. https://doi.org/10.1190/int-2018-0256.1.
Ribot, A., Bossi, J., Cingolani, C.A., Piñeyro, D., 2005. Caracterización petrográfica de la faja milonítica Colonia-Arroyo Pavón en el Sur del Terreno Piedra Alta, Uruguay: Zona de cizalla principal en basamento precámbrico? Actas 16° Congreso Geológico Argentino. 789 (La Plata).
Riccomini, C., Velázquez, V.F., Gomes, C.B., 2005. Tectonic controls of the Mesozoic and Cenozoic alkaline magmatism in central-southeastern Brazilian Platform. In: Mesozoic to Cenozoic Alkaline Magmatism in the Brazilian Platform. 123. pp. 31–56.
Rossello, E.A., De Santa Ana, H., Veroslavsky, G., 2000. El lineamiento Santa Lucia-Aigua-Merin (Uruguay): un corredor tectonico extensivo y transcurrente dextral precursos de la apertura atlantica. Revista Brasileira de Geociências 30, 749–756.
Rossello, E.A., Veroslavsky, G., Masquelin, H., De Santa Ana, H., 2007. El corredor jurocretácico Santa Lucía-Aiguá-Merín (Uruguay): evidencias cinemática transcurrente dextral y controles preexistentes. In: Revista de la Asociacion Geologica Argentina. 62. pp. 92–104.
Rossetti, L.M., Lima, E.F., Waichel, B.L., Scherer, C.M., Barreto, C.J., 2014. Stratigraphical framework of basaltic lavas in Torres Syncline main valley, southern Parana-Etendeka Volcanic Province. J. S. Am. Earth Sci. 56, 409–421. https://doi.org/10.1016/j.jsames.2014.09.025.
Santos, J.O., Chernicoff, C.J., Zappettini, E.O., McNaughton, N.J., Greau, Y., 2017. U-Pb geochronology of Martín García, Sola, and Dos Hermanas Islands (Argentina and Uruguay): Unveiling Rhyacian, Statherian, Ectasian, and Stenian of a forgotten area of the Río de la Plata Craton. J. S. Am. Earth Sci. 80, 207–228.
Santos, J.O.S., Hartmann, L.A., Bossi, J., Campal, N., Schipilov, A., Piñeyro, D., McNaughton, N.J., 2003. Duration of the Transamazonian and its correlation within South America based on U-Pb SHRIMP geochronology of the la Plata Craton, Uruguay. Int. Geol. Rev. 45, 27–48.
Schattner, U., José Lobo, F., López-Quirós, A., dos Passos Nascimento, J.L., de Mahiques, M.M., 2019. What feeds shelf-edge clinoforms over margins deprived of adjacent land sources? An example from southeastern Brazil. Basin Research. https://doi.org/10.1111/bre.12397.
Schmitt, R. da S., Fragoso, R.D.A., Collins, A.S., 2018. Suturing Gondwana in the Cambrian: the orogenic events of the final amalgamation. In: Geology of Southwest Gondwana. Springer International Publishing, pp. 411–432. https://doi.org/10.1007/978-3-319-68920-3_15.
Scotese, C.R., Boucot, A.J., McKerrow, W.S., 1999. Gondwanan palaeogeography and palaeoclimatology. J. Afr. Earth Sci. 28, 99–114.
Shuster, D.L., Flowers, R.M., Farley, K.A., 2006. The influence of natural radiation damage on helium diffusion kinetics in apatite. Earth Planet. Sci. Lett. 249, 148–161. https://doi.org/10.1016/j.epsl.2006.07.028.
Soto, M., Morales, E., Veroslavsky, G., de Santa Ana, H., Ucha, N., Rodríguez, P., 2011. The continental margin of Uruguay: crustal architecture and segmentation. Mar. Pet. Geol. 28, 1676–1689. https://doi.org/10.1016/j.marpetgeo.2011.07.001.
Sprechmann, P., Bossi, J., Da Silva, J., 1981. Cuencas del Jurásico y Cretácico del Uruguay. In: Volkheimer, W., Musacchio (Eds.), Cuencas sedimentarias del Jurásico y Cretácico de América del Sur. 1. pp. 239–270 (Buenos Aires).
Sprechmann, P., Montaña, J., Gaucher, C., 1993. Devónico. In: Bossi, J. (Ed.), Geología y Recursos Minerales del Departamento de Durazno. Intendencia Municipal de Durazno y Cátedra de Geología de la Facultad de Agonomía, Montevideo, pp. 25–55.
Stica, J.M., Zalán, P.V., Ferrari, A.L., 2014. The evolution of rifting on the volcanic margin of the Pelotas Basin and the contextualization of the Paraná–Etendeka LIP in the separation of Gondwana in the South Atlantic. Marine and Petroleum Geology 50, 1–21. https://doi.org/10.1016/j.marpetgeo.2013.10.015.
Stockli, D.F., 2005. Application of low-temperature thermochronometry to extensional tectonic settings. In: Reiners, P.W., Ehlers, T.A. (Eds.), Low-Temperature Thermochronology: Techniques, Interpretations, and Applicationscations. Mineralogical Society of America, pp. 411–448.
Stockli, D.F., Farley, K.A., Dumitru, T.A., 2000. Calibration of the apatite (U-Th)/ He

thermochronometer on an exhumed fault block , White Mountains , California. Geology 28, 983–986. https://doi.org/10.1130/0091-7613(2000)28<983.

Tagami, T., O'Sullivan, P.B., 2005. Fundamentals of fission-track thermochronology. In: Reiners, P.W., Ehlers, T.A. (Eds.), Low-Temperature Thermochronology: Techniques, Interpretations, and Applications. Mineralogical Society of America, pp. 19–48.

Teixeira, W., Renne, P., Bossi, J., Campal, N., D'Agrella, F., 1999. $^{40}Ar/^{39}Ar$ and Rb/Sr geochronology of the Uruguayan dike swarm, Río de la Plata Craton and implications for Proterozoic intraplate activity in western Gondwana. Precambrian Res. 93, 153–180.

Tello Saenz, C.A., Hackspacher, P.C., et al., 2003. Recognition of Cretaceous, Paleocene, and Neogene tectonic reactivation through apatite fission-track analysis in Precambrian areas of southeast Brazil: association with the opening of the south Atlantic Ocean. J. S. Am. Earth Sci. 15, 765–774. https://doi.org/10.1016/S0895-9811(02)00131-1.

Turner, S., Regelous, M., et al., 1994. Magmatism and continental break-up in the South Atlantic. Earth Planet. Sci. Lett. 121, 333–348. https://doi.org/10.1016/0012-821X(94)90076-0.

Uriz, N.J., Cingolani, C.A., Basei, M.A.S., Blanco, G., Abre, P., Portillo, N.S., Siccardi, A., 2016. Provenance and paleogeography of the Devonian Durazno Group, southern Parana Basin in Uruguay. J. S. Am. Earth Sci. 66, 248–267. https://doi.org/10.1016/j.jsames.2016.01.002.

Van Ranst, G., Pedrosa-Soares, A.C., Novo, T., Vermeesch, P., De Grave, J., 2019. New insights from low-temperature thermochronology into the tectonic and geomorphologic evolution of the south-eastern Brazilian highlands and passive margin. Geosci. Front. https://doi.org/10.1016/j.gsf.2019.05.011.

Vermeesch, P., 2009. RadialPlotter: a Java application for fission track, luminescence and other radial plots. Radiation Measurementes 409–410. http://www.ucl.ac.uk/~ucfbpve/radialplotter/.

Veroslavsky, G., De Santa Ana, H., Rossello, E., 2004. Depósitos del Jurásico y Cretácico temprano de la región meridional de Uruguay. In: Veroslavsky, G., Ubilla, M., Martínez, S. (Eds.), Cuencas sedimentarias de Uruguay. Mesozoico. Facultad de Ciencias, Montevideo, pp. 117–142.

Wagner, G.A., Gleadow, A.J.W., Fitzgerald, P.G., 1989. The significance of the partial annealing zone in apatite fission-track analysis: projected track length measurements and uplift chronology of the transantarctic mountains. Chemical Geology: Isotope Geoscience section 79, 295–305. https://doi.org/10.1016/0168-9622(89)90035-3.

Weisberg, W.R., Metcalf, J.R., Flowers, R.M., 2018. Distinguishing slow cooling versus multiphase cooling and heating in zircon and apatite (U-Th)/He datasets: the case of the McClure Mountain syenite standard. Chem. Geol. 485, 90–99.

Wildman, M., Brown, R., Beucher, R., Persano, C., Stuart, F., Gallagher, K., Schwanethal, J., Carter, A., 2016. The chronology and tectonic style of landscape evolution along the elevated Atlantic continental margin of South Africa resolved by joint apatite fission track and (U-Th-Sm)/He thermochronology. Tectonics 35 (3), 511–545. https://doi.org/10.1002/2015TC004042.

Will, T., Gaucher, C., Ling, X.X., Li, X.H., Li, Q.L., Frimmel, H.E., 2019. Neoproterozoic magmatic and metamorphic events in the Cuchilla Dionisio Terrane, Uruguay, and possible correlations across the South Atlantic. Precambrian Res. 320, 303–322.

Will, T.M., Frimmel, H.E., 2018. Where does a continent prefer to break up? Some lessons from the South Atlantic margins. Gondwana Res. 53, 9–19. https://doi.org/10.1016/j.gr.2017.04.014.

Willett, C.D., Fox, M., Shuster, D.L., 2017. A helium-based model for the effects of radiation damage annealing on helium diffusion kinetics in apatite. Earth Planet. Sci. Lett. 477, 195–204.

Wolf, R.A., Farley, K.A., Silver, L.T., 1996. Helium diffusion and low-temperature thermochronometry of apatite. Geochim. Cosmochim. Acta 60, 4231–4240. https://doi.org/10.1016/S0016-7037(96)00192-5.

Wolf, R.A., Farley, K.A., Kass, D.M., 1998. Modeling of the temperature sensitivity of the apatite (U-Th)/He thermochronometer. Chem. Geol. 148, 105–114. https://doi.org/10.1016/S0009-2541(98)00024-2.

Zalán, P.V., 2004. Evolução Fanerozóica das Bacias Sedimentares Brasileiras. In: Mantesso-Neto, V., Bartorelli, A., Carneiro, C.D.R., Neves, B.B. de B. (Eds.), Geologia Do Continente Sul-Americano: Evolução Da Obra de Fernando Flávio Marques de Almeida. Beca Produções Culturais Ltda, pp. 595–612.

Zambrano, J.J., Urien, C.M., 1970. Geological outline of the basins in southern Argentina and their continuation off the Atlantic shore. J. Geophys. Res. 75, 1363–1396. https://doi.org/10.1029/JB075i008p01363.

Zerfass, H., Chemale, F., Leandro, C., Lavina, E., 2004. Tectonics and Sedimentation in Southern South America During Triassic. 166. pp. 265–292. https://doi.org/10.1016/j.sedgeo.2003.12.008.